UNIVERSITY OF LIVERPOOL

The Magnetic fields of Uranus and Neptune from Voyager Data.

A thesis presented by:

Henry Morten

to the department of Earth, Ocean, and Ecological Sciences,
in partial fulfilment of the requirements
for the degree of Bachelor of Earth Science
in the Subject of
Geophysics (Physics).
University of Liverpool,
April 2023.

Supervised by Professor Richard Holme

Declaration:

I, **Henry Morten**, confirm that the work submitted in this dissertation is my own, and that appropriate credit has been given where reference is made to the work of others.

Signature: ***hmorten***

Date: **19/04/2023**

Abstract:

We constrain one of the most fundamental, and recently contested physical properties of both Uranus and Neptune, their rotational periods. We compare the fit to the data provided by the Voyager 2 magnetic field experiment, through a range of rotational periods for both planets to derive their optimal rotation periods.

Slower rotational periods for both Uranus and Neptune (+ 2hrs 2min, and + 10min respectively) were found to maximise the fit to the available magnetic data. We compare these findings to the currently accepted rotational periods of both planets, and periods defined by Nettelmann et al. (2012), who have derived periods from long term observations of the planets satellite motions (-40 min, and +1hr 20 min respectively).

We present a variety of new magnetic field models for both planets, over the outlined rotational periods. We find the simplest models that satisfy the data, and use both the surface heat flow, and an Ohmic heating constraint on the magnetic field structure at varying depths within each planet.

There is a considerable difference in the fit to data, and the overall field structure for the magnetic fields generated by the different rotational periods of Uranus. The period derived in this thesis resolving more field structure and providing a closer fit to data, than the currently accepted rotational period.

Potential causes for difference in derived rotational periods are discussed, along with the dangers of non-uniqueness in our models. Discrepancies between different datasets used to construct magnetic field models of Uranus are also discovered.

The field models of Neptune are more consistent across the different rotational periods. Some additional short wavelength features are present in models generated from the period of Nettelman et al. (2012), with an increase in the misfit to data.

Table of Contents:

Figures:

Chapter 1 - Introduction:

1.1 Uranus, Neptune, and their place in the Solar System:

Lurking in the furthest reaches of our solar system lie the two planets, Uranus, and Neptune. Both planets have respective magnetic fields that are equally like each other, and unlike any of the other known magnetised planets (Connerney, 1993). The fields of Earth, Mercury, Jupiter and Saturn are all dominantly dipolar, with strong (or near perfect in the case of Saturn) symmetry about the rotation axis (Holme and Bloxham, 1996). Mars appears to have once had an ancient planetary dynamo. Venus does not currently have a significant planetary magnetic field and the resulting high surface temperatures on the planet should have prevented the recording of any evidence of any ancient magnetic field (Russell, 1993).
These contrast starkly from the magnetic fields of Uranus and Neptune. So far only one set of in situ measurements of the planetary magnetic fields of both planets have been taken, which took place on the 24th January 1986 for Uranus and 24th August 1989 for Neptune by Voyager 2 (Ness, 1993, 1989).

Voyager 2 was an advanced spacecraft, launched on the 20th August 1977, a time during which it was most favourable for reaching Saturn by a gravity-assisted flypast of Jupiter; reducing the total launch energy demands (Kohlhase and Penzo, 1977). The Voyager 2 spacecraft was launched primarily to explore the Jovian and Saturnian planetary systems, as well interplanetary space. The Voyager Mission description documentation describes only "a possible continuation on to Uranus", after a gravity-assist swing-by of Saturn, for the second arriving Voyager spacecraft (Kohlhase and Penzo, 1977, p1). Flight paths for the Voyager 2 encounters about both planets can be seen in figure *(1)*, where the proximity of Voyager 2 to the northern hemisphere of Neptune is noted, causing that hemisphere to be more accurately constrained.

In this report, it should be noted that the coordinate system used is identical to that adopted by Ness et al. (1986). This is a West - Longitude coordinate system whereby longitude as viewed by a stationary observer increases with time. All following figures and references will be with respect to this coordinate system. Later in this report, we will look at changing the rate of

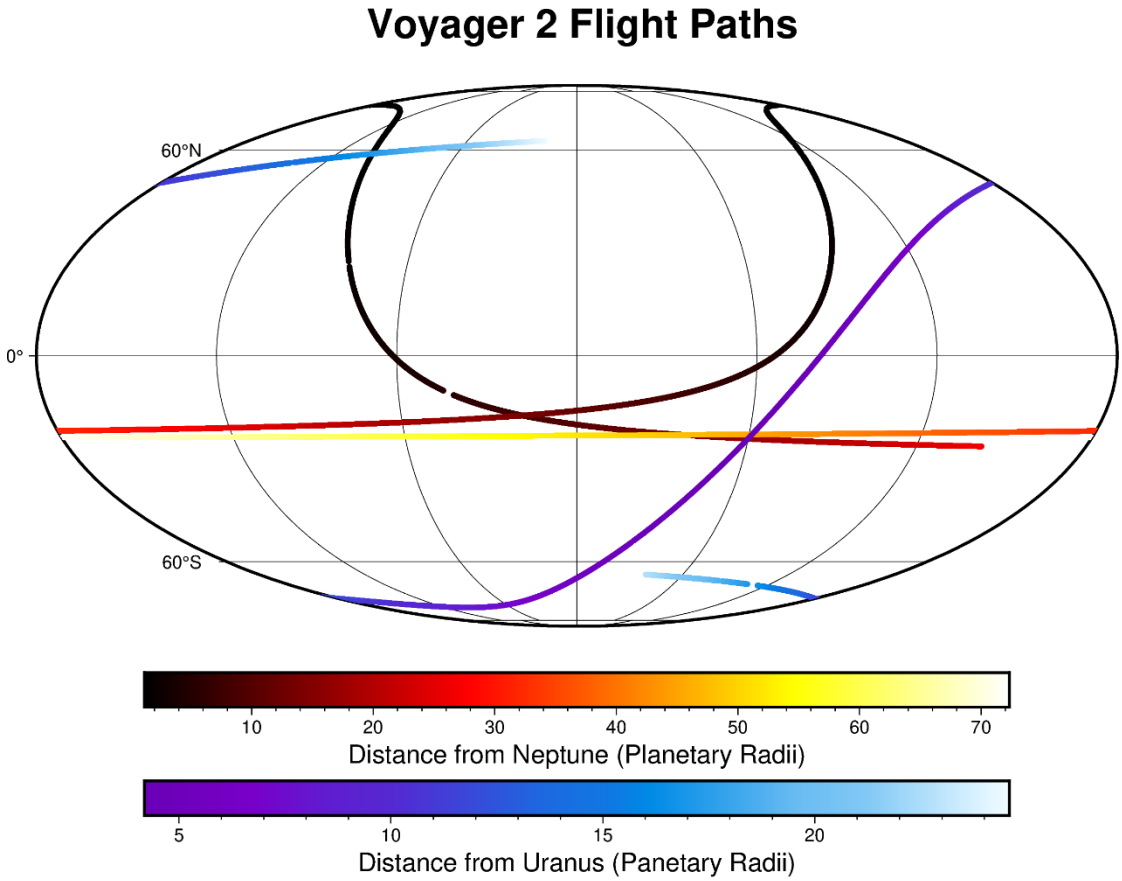

Figure 1: *Orbital flight paths of Voyager 2 about both Uranus and Neptune, the map has been produced using the PyGMT Software (Uieda, Leonardo et al., 2022) – representing all positional data we have available, plotted in a West Longitude Coordinate system.*

change of longitude with respect to a fixed change in time to the rotation period of both planets, we artificially change the accepted rotation rate, and compare the fit to data for the different times, comparing to recent work performed by Nettelmann et al. (2012), who have argued for the change in accepted rotation of the planets.

Uranus and Neptune reside at a mean orbital distance of 19.2 and 30 AU (Astronomical Units) respectively, and are the most distant of planets in our Solar System (Connerney, 1993). They are known to be similar in size to one another (approximate radius of 25,000 km), have mass of about $15M_E$ (Earth masses), and presumed compositions of largely low-temperature condensates (Connerney, 1993). Neither planet was known to have a magnetic field of their own. The very first radio emissions were not detected or recognised until just prior to Voyager 2's entry into the relevant magnetosphere (Desch et al., 1991; Gurnett et al., 1989). This is due to the weak and low frequency emissions from the planets, for Neptune the spacecraft did not detect any radio emissions at low frequencies (<100 kHz) until a few days before the closest approach.

Voyager 2 was fitted with a wide range of equipment, but those of special interest are the magnetometers. Carried on both missions were dual low field (LFM) and high field magnetometer (HFM) systems which switched automatically between ranges of sensitivity. The benefit of the dual systems was to provide a greater reliability of measurements and, in the special case of the LFM's, they allow the separation of spacecraft magnetic fields from the ambient fields (Behannon et al., 1977).

1.2 Planetary Interior:

Despite the two planets being known as "icy planets", there appears to be no such evidence that they actually consist of significant amounts of ices (Helled et al., 2010).

Relatively little is known about the interior structure and composition of the two planets. One general conclusion appears secure, in that Uranus and Neptune differ substantially in bulk composition from Jupiter and Saturn – being made predominantly of denser material than that of bulk hydrogen composition (Hubbard and MacFarlane, 1980). Uranus is composed of a mixture of rock (mainly SiO_2), being a mix of Hydrogen and Helium, with Neptune a mix of ice (H_2O) with solar Hydrogen and Helium (Helled et al., 2010).

1.3 Magnetic Fields:

1.3.1 Uranus:

Upon Voyager 2's entry into the Uranian magnetosphere, the observed magnetic field magnitude was approximately 7 nT. The observed field magnitude then steadily increased to a maximum of 413 nT, just two minutes before closest approach (Ness et al., 1986). The most exciting result of the Voyager magnetic investigation of Uranus was the extraordinarily large angular separation between the dipole and rotational axes, being approximately 60° (Connerney et al., 1987). This can be seen in figure *(2)*, a diagram of an offset tilted dipole (OTD), representative of Uranus. This result was obtained by spherical harmonic analysis to first order in internal terms (centred internal dipole), and to first order in external terms (uniform external field) (Ness et al., 1986). The true magnetic field of Uranus is however more complex than the OTD model introduced below, having more higher degree components than the closer planets (Connerney et al., 1987; Ness et al., 1991).

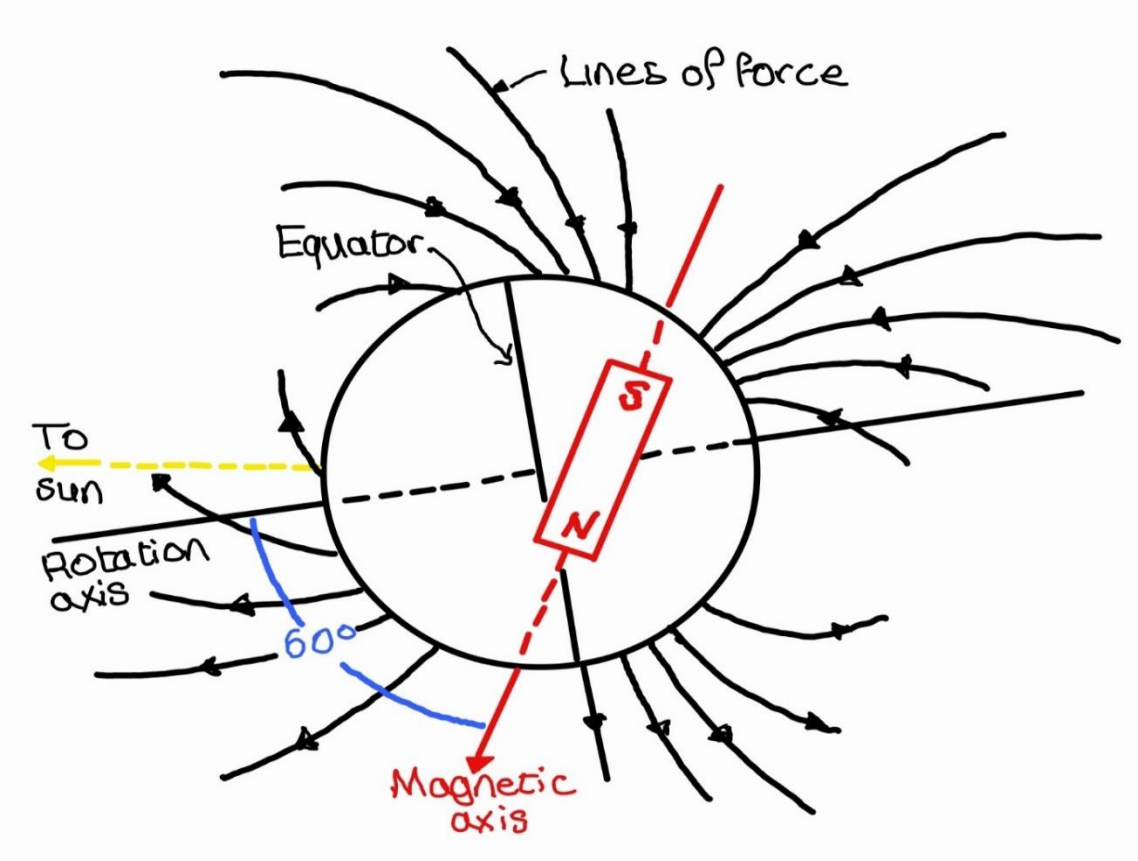

Figure 2: *Diagram of the offset tilted dipole (OTD), with a large angular and spatial offset from the rotation axis of Uranus. Adapted from (Ness et al., 1986).*

1.3.2 Neptune:

Upon Voyager 2's entry into the magnetosphere of Neptune, the observed magnitude of the magnetic field was between 1 and 2 nT, the field then increased steadily, reaching a maximum of 9,950 nT, just before Voyagers closest approach of Neptune at $1.18R_N$ (Radius of Neptune). The field then steadily decreased with increasing radial distance from the planet, dropping back to 1 nT at $24R_N$ (Ness et al., 1989). As seen in figure *(3)*, there is, along with Uranus, an offset angle present when the planet is represented as an OTD - this planetary magnetic field appears similar in many ways to that of Uranus. For both planets, this OTD representation of the magnetic field is a useful tool for visualizing the essential characteristics of the field, and for describing the motion of charged particles,

throughout much of the planet's magnetosphere. This is particularly useful at larger radial distances from the planet (Connerney et al., 1991).

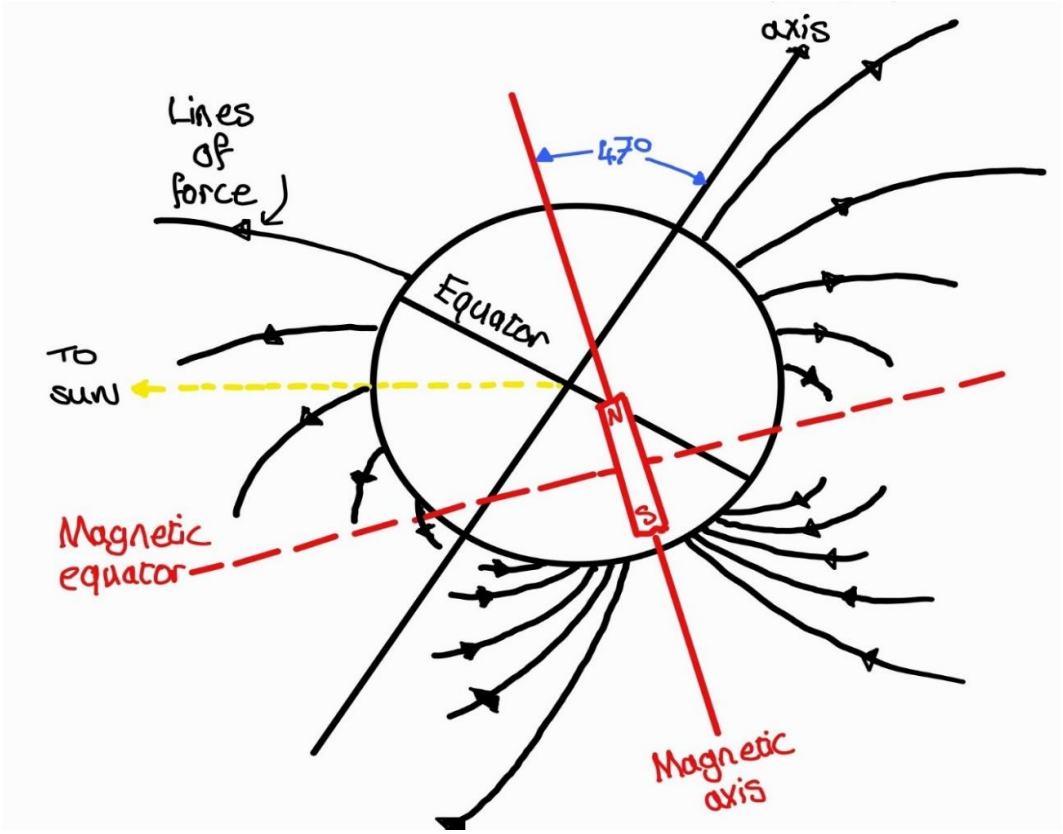

Figure 3: *Diagram of the offset tilted dipole (OTD), with a large angular and spatial offset from the rotation axis of Neptune. Adapted from (Ness et al., 1989).*

1.3 Project Motivation:

The motivation for this project has come about because of fairly recent work published by Nettelmann et al. (2012) and Neuenschwander and Helled (2022) who have argued that the rotation periods of both planets should be different to the currently accepted values. They claim since the Voyager fly-bys of Uranus and Neptune, improved gravity field data have been derived from long-term observations of the planets' satellite motions, and modified shape and solid-body rotation periods have been suggested. A 40 minute faster rotation period for Uranus and a 1 hour 20 minute slower rotation period for Neptune compared to the Voyager data are preferred (Nettelmann et al., 2012). Through this project, accurate magnetic field models are going to be constructed for both planets, and we're going to investigate the effects of artificially altering the rotation rates of both planets. Comparisons will then be made between the fit to data of the respective magnetic field models.

Chapter 2 - Methodology:

2.1 Modelling the Planetary Magnetic Field:

A dipole is the simplest type of feasible potential field, and also happens to be the configuration of a magnetized uniform sphere. This is defined from Gauss's law for magnetism, whereby the magnetic flux, **B**, across any closed surface is zero:

$$\nabla \cdot \boldsymbol{B} = \mathbf{0} \tag{1}$$

We can continue to express the magnetic field of a planet from the differential form of Ampère's law:

$$\nabla \wedge \boldsymbol{B} = \mu_0 \boldsymbol{J} \tag{2}$$

In which the curl of the magnetic field at any point, is the same as the current density at that same point (μ_0 being the permeability of free space). When there are no sources, $\boldsymbol{J=0}$, and the curl of $\boldsymbol{B=0}$. Thus, the magnetic field, $\boldsymbol{B}$, of a planet in an electrical insulator can be determined by the negative gradient of a magnetic scalar potential, as follows:

$$\boldsymbol{B}(r, \theta, \phi) = -\nabla V(r, \theta, \phi) \tag{3}$$

Which, from knowledge regarding Gauss' law for magnetism, any magnetic scalar potentials have to satisfy Laplace's equation:

$$\nabla \cdot \boldsymbol{B} = \nabla^2 V(r, \theta, \phi) = \mathbf{0} \tag{4}$$

A more traditional solution for a planetary magnetic field can be expressed in spherical geometry (Langel, 1988):

$$V(r, \theta, \phi) = \sum_{n=1}^{\infty} \left\{ \left(\frac{r}{a}\right)^n T_n^e + \left(\frac{a}{r}\right)^n T_n^i \right\} \tag{5}$$

Where a is the equatorial radius of the planet, and (r, θ, ϕ) is a planetocentric coordinate system.

With the first series in increasing powers of $\boldsymbol{r}$, representing external sources to the magnetic field, with:

$$\boldsymbol{T_n^e = \sum_{m=0}^{n} P_n^m cos(\theta)\,[G_n^m\, cos(m\phi) + H_l^m\, sin(m\phi)]}$$

6

The second series are contributions due to the internal planetary field with:

$$\boldsymbol{T_n^i = \sum_{m=0}^{n} P_n^m cos(\theta)\,[g_n^m\, cos(m\phi) + h_l^m\, sin(m\phi)]}$$

7

$\boldsymbol{P_l^m cos\,(\theta)}$ are Legendre polynomials, by convention Schmidt normalised (Holme and Bloxham, 1996):

$$\boldsymbol{\int_{\phi=0}^{2\pi}\int_{\theta=0}^{\pi}(P_l^m cos\,(\theta) cos\,(m\phi))^2\, sin(\theta)\, d\theta d\phi = \frac{4\pi}{2l+1}}$$

8

The measurements of the magnetic field can be used to estimate values of $[\boldsymbol{g_l^m, h_l^m, G_l^m, H_l^m}]$, which are the internal and external Gauss coefficients respectively – which uniquely define the planets external magnetic field down to the source of the field (Holme and Bloxham, 1996).

2.1.2 The external magnetic field of Uranus:

In this report, we are following the convention as determined by Connerney et al. (1991, 1987) for the calculation of the magnetic fields of Uranus and Neptune.

For Uranus, both the internal and external Gauss coefficients are calculated to a sufficiently large magnitude to represent the observed field, but not so large as to introduce more free parameters than can be accurately determined by the observations (the number of free parameters in each of the series grows rapidly with N, as $n_p = (N+1)^2$ - 1) (Connerney et al., 1987).

For Neptune, no external Gauss coefficients have been calculated as the external expansion may be truncated at $n = N_{MAX} = 1$, which corresponds to the uniform external field which is present, due to distant magnetopause and tail currents (Connerney et al., 1991).

2.2 Selection of Data, and its retrieval:

All data has been acquired from the NASA Planetary Data System (PDS) (https://pds.nasa.gov/). While both planets are fundamentally quite similar and the same spacecraft has been used for the acquisition of all data used to model the magnetic fields, the process in which data was collected was fundamentally different.

2.2.2 Neptune:

For Neptune, we are building on the extensive work carried out by Connerney et al. (1991) where, as part of the PDS data for Neptune in the NLS (**N**eptune **L**ongitude **S**ystem) coordinate system (Ness, 1989), they have already collated data as a subset of the Voyager 2 vector magnetic field observations obtained within $12R_N$. This aimed to achieve the highest temporal resolution possible from the available data.

Voyager 2 was in the magnetosphere of Neptune for 38 hours, during which, three orthogonal components of the magnetic field $(\hat{\boldsymbol{r}}, \hat{\boldsymbol{\theta}}, \hat{\boldsymbol{\phi}})$ were recorded without any major interruption (Holme and Bloxham, 1996). The instrumentation available on Voyager 2, included both the LFM and HFM magnetometers, both of which respond to different magnitudes of magnetic field and were both used during the encounter with Neptune (Behannon et al., 1977).

2.2.3 Uranus:

For Uranus, there were several complications. We initially used data from the 1.92 second time averaged section (averaged from the 60 ms instrument sample rate) – which is available in U1 (Uranus Longitude) coordinates. This data was selected as it provides the greatest temporal resolution possible from those available. However, the positional information (Longitude, and Latitude) had no resemblance to the actual flight path of Voyager 2. This can be seen in figure *(4)*, where there is some attempt at a possible flight path, but the rest of the data is seemingly incomprehensible noise; therefore, some form of interpolation has to be made between the 1.92 second magnetic data, and positional data that has been time averaged over a longer time period in order to retain the temporal resolution. A further step is for the removal of appropriate 'Data contamination flags' from the Uranus data set, as defined by Ness (1993):

"Flag, a character string which indicates software or s/c hardware intervention which reduces confidence in the data (NULL flags represent 'good' data)."

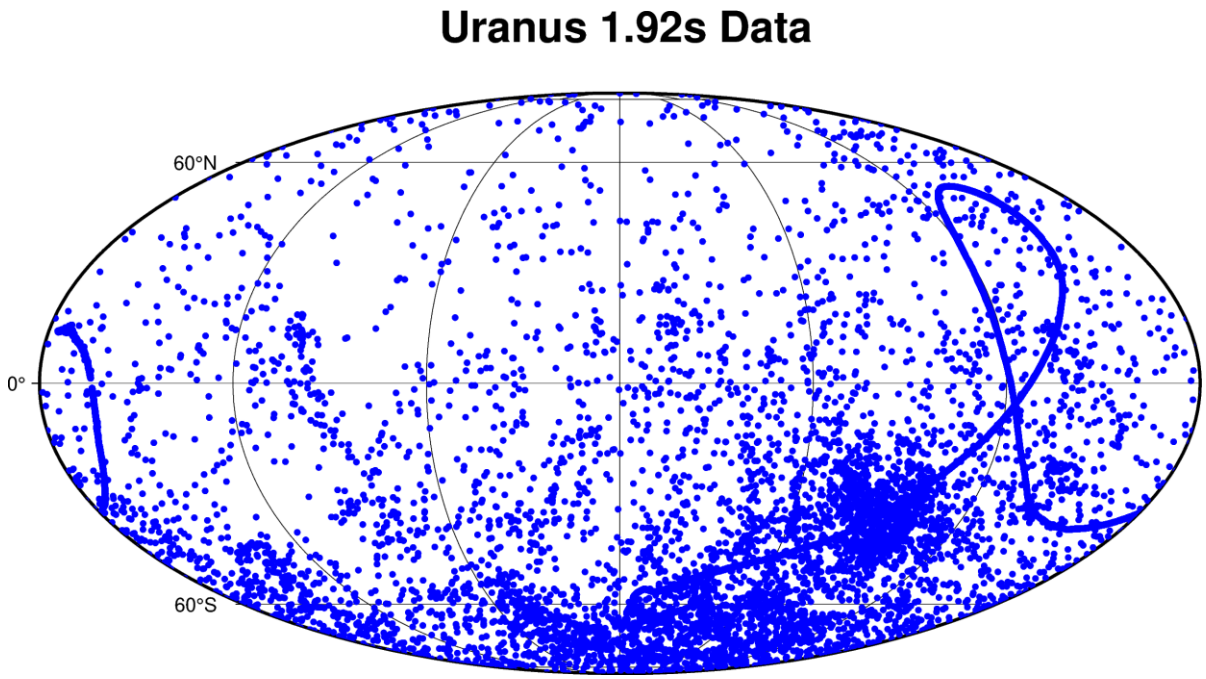

Figure 4: *1.92 second time averaged data, regarding Voyager 2's supposed flight path about Uranus. The map has been produced using the PyGMT Software (Uieda, Leonardo et al., 2022), plotted in a West Longitude Coordinate system.*

2.2.4 Time series analysis using Splines (smoothing):

There are separate (correct) positional data available for the Voyager 2 encounter with Uranus in U1 coordinates, sampled every 48 seconds. As we wish to have the highest possible temporal resolution, we determine a continuous running average for each of the positional arguments (Latitude, Longitude, Planetary distance between Uranus and Voyager 2) by the use of fitting a smooth curve through each component using penalized least squares splines (Constable and Parker, 1991, 1988). We aim to find the smoothest function $\boldsymbol{f(x)}$ which provides a fit to the data $\{\boldsymbol{y_i}\}$, standard deviation $\{\boldsymbol{\sigma_i}\}$, by minimising:

$$\boldsymbol{F} = \sum_{\boldsymbol{i=1}}^{\boldsymbol{N}} \frac{(\boldsymbol{y_i} - \boldsymbol{f(x_i)})^2}{\boldsymbol{\sigma_i^2}} + \boldsymbol{\lambda} \int \boldsymbol{f''(x)^2 dx} \quad (9)$$

The solution to this is a set of piecewise cubic polynomials, which are called smoothing splines, joined at the locations of the datapoints $\{\boldsymbol{x_i}\}$, named knots. For a large number of data, the calculation of these functions becomes problematic (Holme and Bloxham, 1996).

Constable and Parker (1988) suggested an alternative method, named penalized least squares splines, based on a construction of a more widely spaced sequence of knots, $\boldsymbol{x_k}$, upon the smoothing function is constructed on a basis of B-splines (Holme and Bloxham, 1996). An example of this is shown in figure *(5).*

The closeness of fit from the B-Spline to the data is controlled by a damping parameter – as

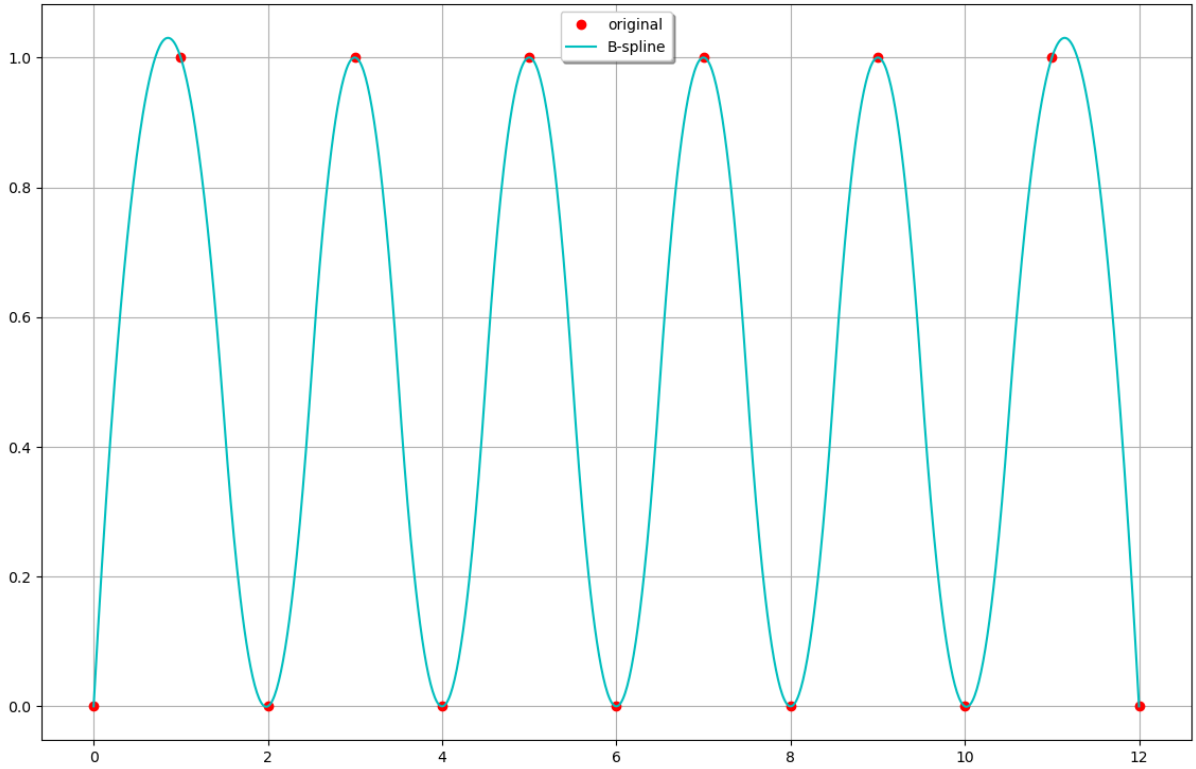

Figure 5: *A - B spline basis of evenly spaced knots (Red datapoints) - with a B-Spline basis joining the points. Figure generated using: (Hunter, 2007).*

will be further elaborated on in **section 2.3.4.** A smaller damping parameter allows for a closer fit to data with more variation, whereas a larger damping parameter produces a smoother function with a larger misfit.

A trade-off for different damping parameters has been generated for the B-Spline fit and can be seen in figure *(6).* A damping parameter of $\mathbf{1 \times 10^5}$ has been selected and, in turn, each of the Spline curves is matched to a second time series of resolution 1.92 seconds (the same as the magnetic field data). This allows the construction of spacecraft positional data at the same temporal resolution.

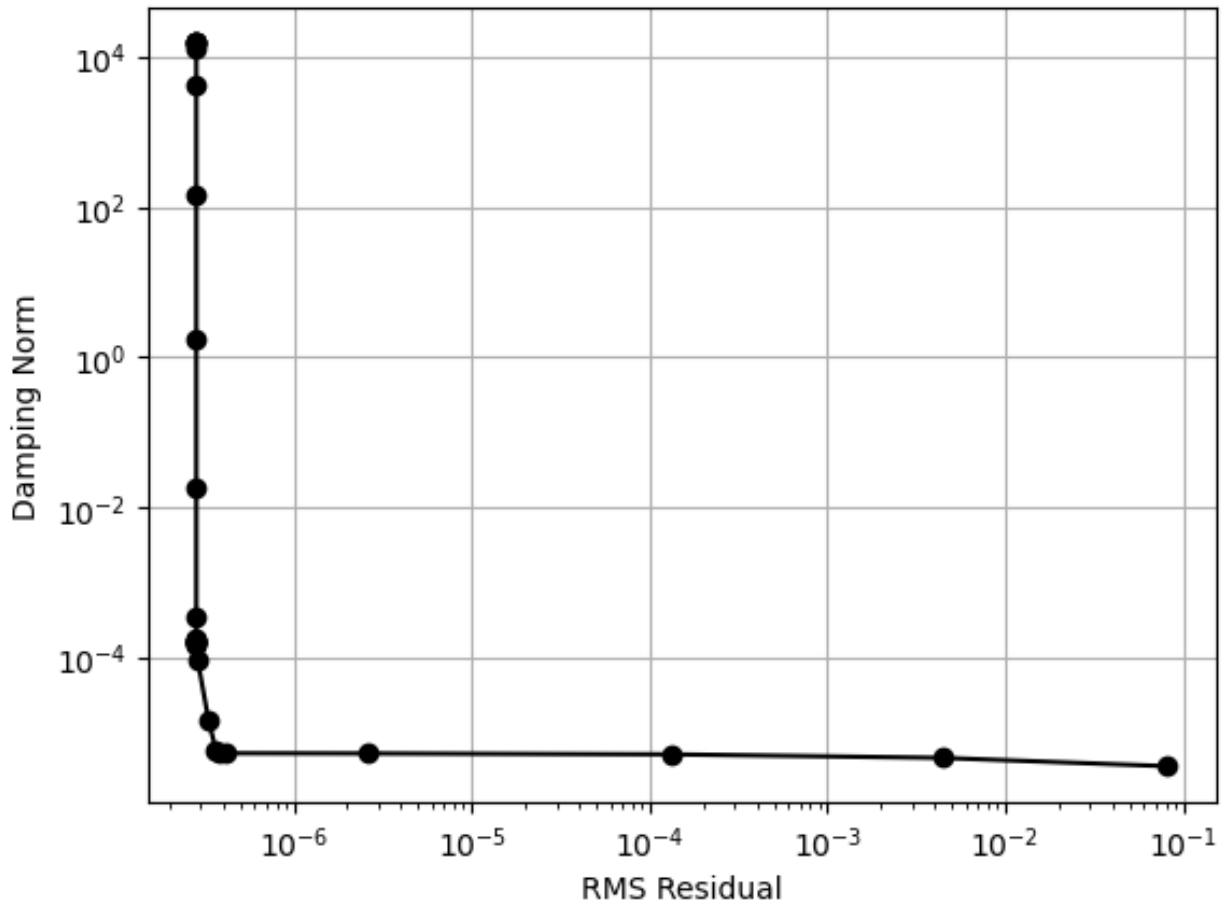

Figure 6: *Trade off curve for different damping parameters for the B-Spline fit. Figure generated using: (Hunter, 2007)*

2.3 Inverse Theory:

The aim of this report is to determine appropriate magnetic field models of Uranus and Neptune from the available data. From equation *(5)* one possible approach would be of determining Gauss coefficients:

$$\boldsymbol{m} = \{\boldsymbol{g_1^0}, \boldsymbol{g_1^1}, \boldsymbol{h_1^0}, \boldsymbol{g_2^0}, \boldsymbol{g_2^1} \ldots\} \tag{10}$$

which uniquely define the planetary magnetic field external to the source region in the planet (Holme and Bloxham, 1996).

In order to create an infinitely detailed model of a magnetic field, we need an infinite amount of data to contribute to the construction of the model. As Voyager 2 is the only spacecraft to visit both of the planets, and has conducted only one fly-by of each, we only have a very limited amount of data to construct models from.

Here in lies our primary issue of '*non-uniqueness'* whereby there are a large variety of magnetic field models that would be able to satisfy the finite data we have available, and as a result we have an under-determined problem.

2.3.2 Model Vector:

Gauss coefficients are the parameters that are solutions to the model vector, and can be determined using:

$$\boldsymbol{\gamma} = \boldsymbol{Am} + \boldsymbol{e}$$

11

With $\boldsymbol{\gamma}$ being the data vector, **m** the model vector and $\boldsymbol{A}$ being a matrix that relates the two, and $\boldsymbol{e}$ representing the vector of errors. To solve this, we are using the least squares approach to try and minimise the sum of squares on the errors, where:

$$\boldsymbol{A^T Am} = \boldsymbol{A^T \gamma}$$

12

This leads to the least squares solution being precisely our generalised inverse matrix formalism. If the matrix $\boldsymbol{A^T A}$ is singular and non-invertible, it leads to a problem of "null space" where any associated vector yields no information on the problem and has no effect on the data.

2.3.3 Error Matrix:

If the errors on the data are assumed to be Gaussian, with a zero mean, in order to optimise the fit to the representative data, we should aim to minimise (Holme and Bloxham, 1996):

$$\boldsymbol{e^T C_e^{-1} e}$$

13

Where $C_e$is the data covariance matrix for the errors and the error in terms of **e**, is defined by the re-arranging of equation *(11)*. We assume all the data are linearly related to the model. Following this, the maximum likelihood solution is:

$$\boldsymbol{\widehat{m} = (A^T C_e^{-1} A + \lambda \Lambda)^{-1} A^T C_e^{-1} \gamma}$$

14

where $\boldsymbol{\lambda}$ is a Lagrange multiplier and the matrix $(\boldsymbol{A^T C_e^{-1} A + \Lambda \lambda})$ is a real, symmetric and positive definite. The solution to equation *(14)* can be obtained efficiently by methods such as Cholesky Decomposition (used in this case). Cholesky decomposition is a special case of

Lower Upper decomposition where the matrix is symmetrical and the upper triangular matrix is a transpose of the lower triangular matrix, exploiting the emergence of patterns that arise when determining a solution.

2.3.4 Regularization (Damping):

Regularization is a method of simplifying models, by controlling (or "regulating") the amount of small scale, short wavelength features that are allowed through from the data to the model. We are adding a matrix to the normal equations matrix to control instability, through the damped least-squares solution:

$$(\boldsymbol{A^T A + \mu I})\boldsymbol{m} = \boldsymbol{A^T \gamma}$$

15

Where $\boldsymbol{\mu}$ = The damping parameter, and $\mathbf{I}$ =The identity matrix.

A larger damping parameter increases numerical stability compared to other models. Small eigen-vectored eigenvalues produce instability by allowing too much of a contribution from short wavelength noise through into the model, and zero eigenvalues contribute to non-uniqueness. Adding a constant value to all eigenvalues increases their stability, and reduces their errors, as we are forcing all eigenvalues to be larger, and diverge from 0.

The larger the damping parameter, the less of a contribution short wavelength features make to the model, making it controlled by longer wavelength features.

The first application of a damping parameter can be seen earlier in figure *(6)*. Too large of a damping parameter creates a Residual (misfit to data) value that is too large – a location that is far from the origin on the x-axis. Too small of a damping parameter starts increasing the distance from the origin on the y-axis, making the model increasingly more complex, being dominated by sort wavelength features with little or no improvement of the model fit to the data. Therefore, the optimal damping parameter is one that is both optimally smooth and fits the data – described as the "knee", or the turning point in the line in figure *(6).* This technique can sometimes be problematic when there is no clear or definitive turning point in the trade off curve generated by the data.

Regularization will be applied with respect to two different constraints, with regards to the smoothing norm at the surface of each planet and the ohmic heating norm at the expected depth of field generation: 0.75 R_U, and 0.8 R_N (Holme and Bloxham, 1996).

Following work done by Shure et al. (1982), we seek fields which are smooth over a volume or a surface.

We can express this quantity, along with others that are similar to it, as a quadratic norm:

$$\boldsymbol{m^T \Lambda m}$$

16

Where $\boldsymbol{\Lambda}$ is a positive definite matrix, with diagonal elements:

$$\boldsymbol{f(l,r) = (l+1)\left(\frac{a}{r}\right)^{2l+4}}$$

17

And zeros elsewhere (Holme and Bloxham, 1996). Where we then minimize:

$$\boldsymbol{(\gamma - Am)^T C_e^{-1} (\gamma - Am) + \lambda m^T \Lambda m}$$

18

Where $\boldsymbol{\lambda}$ is a Lagrange multiplier. The extent to which the field model is determined by the data is described by the resolution matrix:

$$\boldsymbol{R = (A^T C_e^{-1} A + \lambda \Lambda)^{-1} A^T C_e^{-1} A}$$

19

If $\boldsymbol{\lambda}$ is very small, all parameters are determined by solely by the data.

2.4 Spectral Analysis:

Along with creating respective field models for both planets, the power spectrum provides an alternative insight into the magnetic field. The power spectrum is a way of visualising the contribution of the mean square field (in nT), used by Lowes (1974) with respect to each harmonic degree (**l**) (truncated to degree 16). The power contribution of each harmonic degree to the overall field is given by:

$$\boldsymbol{P(l,r) = (l+1)\left(\frac{a}{r}\right)^{2l+4} \sum_{m=0}^{l} [(g_l^m)^2 + (h_l^m)^2]}$$

20

When the power spectrum plateaus, at increasing harmonic order, the spectrum is described as being "white". A white spectrum is an indicator that different parts of the power spectrum have equivalent amplitude or a similar contribution to the total magnetic field.

It has been shown at the Earth's surface the power spectrum whitens at approximately ***l=14*** (with higher order ***l*** being assumed to be dominated by lithospheric sources) (Holme and Bloxham, 1996).

There has been speculation that the same procedure can be applied to non-Earth fields. If depth can be found at which the spectrum is close to white, this depth could be related to the source region for the field (Holme and Bloxham, 1996). The conversion between harmonic order and the wavelength (or depth to source) can be achieved relatively simply (Maus, 2008):

$$\boldsymbol{\lambda = \frac{2\pi r}{l + 0.5}} \qquad 21$$

Where **λ** is the wavelength, **r** the radius of the planet, and ***l*** is the spherical harmonic degree.

2.5 Errors and their treatment:

When modelling a geomagnetic field, it is generally considered normal to treat all errors on the represented data as being uncorrelated, although this generally far from true. One form of error correlation can be easily dealt with fairly easily – when several pieces of data are measured in the same place, at the same time, all of the data are correlated (Holme, 2000).

In the data set constructed by Connerney et al. (1991) for Neptune, there are individual weighted errors for each vector observation of the internal field in terms of the standard deviation in the observation – insuring that each residual is compared to its expected error (Ness, 1989). This is different to Uranus, where each of the errors on the data are assumed to be equal in magnitude, with value of 1.0 nT. Separate errors are also found within the Uranus dataset – whereby there are several anomalous spikes in the magnetic data, as can be seen in figure *(7)*. Where in each of the X,Y,Z components of the data, there is a sharp spike, deviating from the background trend – most notably at the peak of the Y-component.
These have been acknowledged to be attitude errors, as the magnitude of each of the components does not contain the same errors.

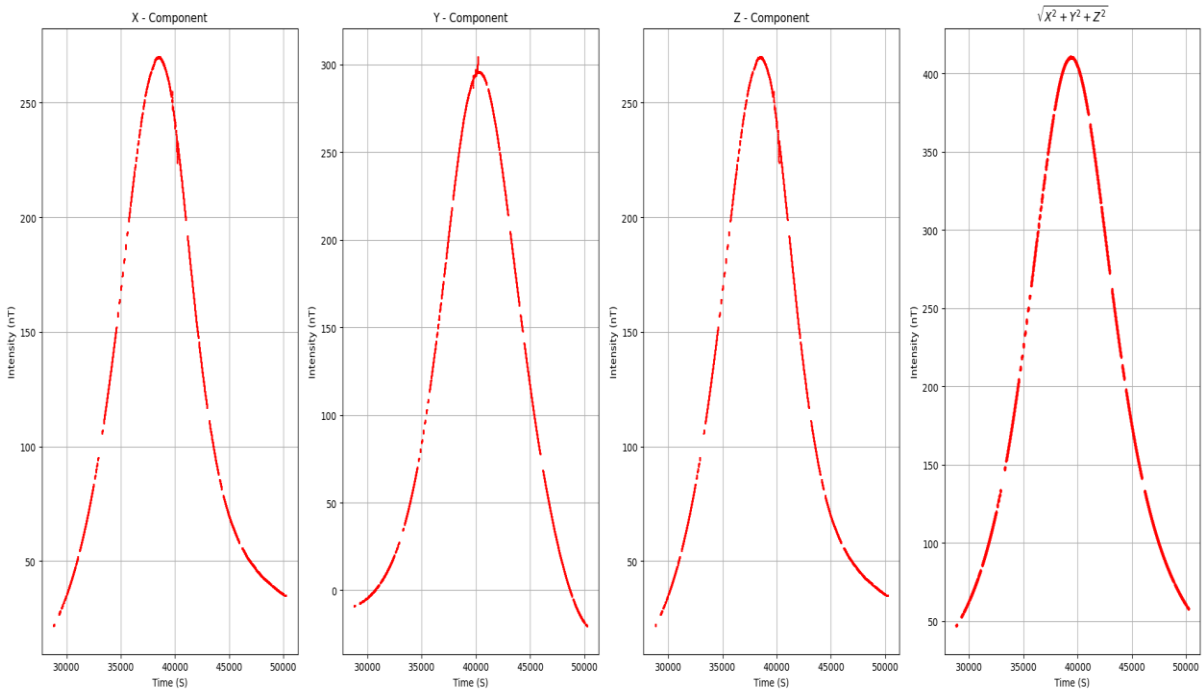

Figure 7: *Visualization of attitude error present for each of the orthogonal components of the magnetic data. Figure created using (Hunter, 2007).*

2.6 Changing Rotation periods:

As mentioned, Nettelmann et al. (2012) have argued for alternate rotational periods of Uranus and Neptune(-40 minutes and +1hr 20 minutes respectively).

We have been able to synthetically alter the rate of change of longitude values for the respective datasets. Longitude measurements, in degrees, are a convolution of the spacecraft velocity, and the angular frequency of the planet.

The currently accepted rotational periods of the two planets (17.24 and 16.11 hours respectively), have been altered in one-minute increments, to $\pm$300 minutes in Python for both planets.

The final longitudes can be visualised in figure *(8).* The code used to achieve this is available in the appendix (functions.py), along with appropriate comments and explanation throughout.

The longitude values at closest approach have been fixed in order to keep the dominant features in the field maps centred in the same place. If the differences in time would have been calculated from the start of the Voyager 2 encounter with the respective planets, the main features on the field maps would have all received a constant shift in longitude.

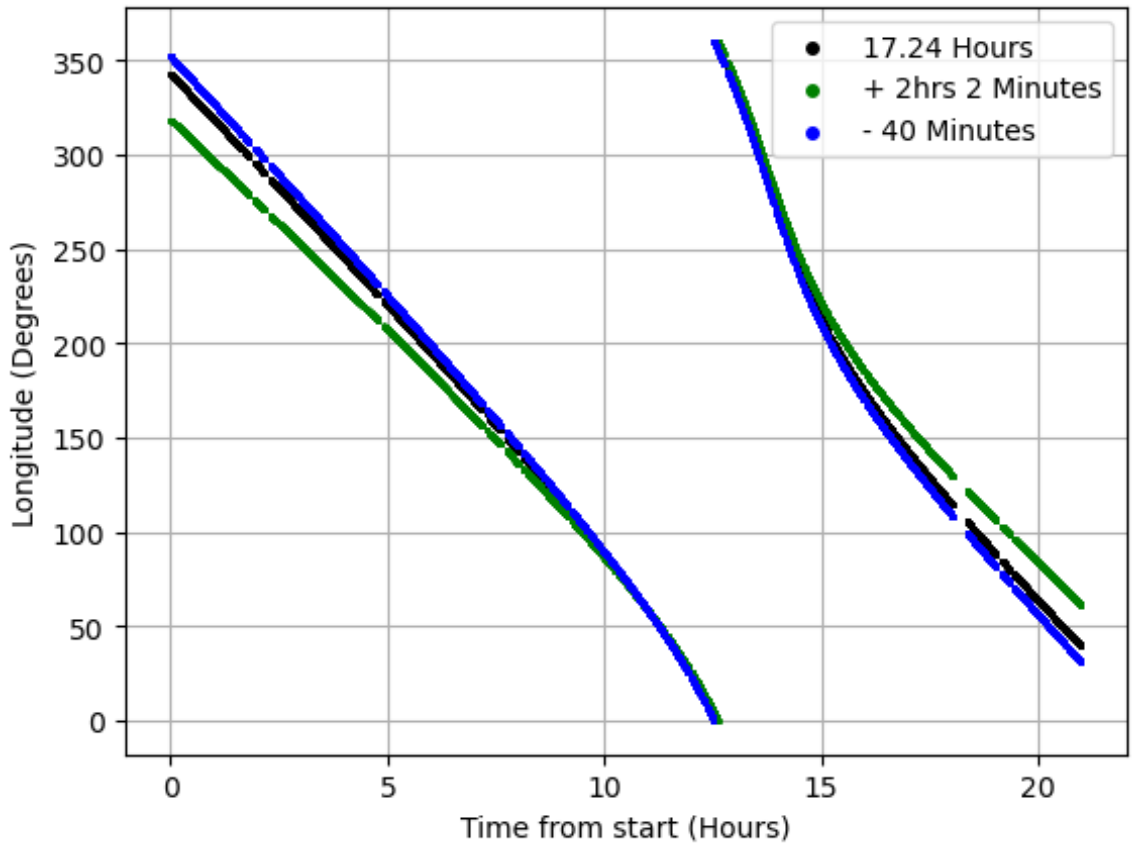

Figure 8: *Changes in longitudes for Uranus. Fixed longitude at closest approach, with longitudes deviating the further you are from that time. Figure has been generated using (Hunter, 2007).*

Further interpolation has to be made for the dataset constructed by Connerney et al. (1991) for Neptune, as no time information were provided.

Interpolation of time data has been achieved in two ways:

1. Initially incorrectly, by determining the amount of datapoints within a full rotation of the planet and extrapolating a 'synthetic' time between each data point by accounting for the currently accepted rotational period of the planet. This has been determined to be approximately 86.56 seconds between datapoints, because of the rate of change of longitude being a convolution of planetary angular frequency and angular velocity.

2. Then correctly, by applying a gap of 48s between data recorded by LFM range 5, 24s sampling interval for LFM range 6, and a 12s sampling interval for HFM observations (Connerney et al., 1991).

Unless stated otherwise, the results have been calculated using the spacing as defined by in technique 2, as that is how Connerney et al. (1991) intended for their data to be constructed.

Chapter 3 – Results and Discussion:

3.1 Choosing ideal rotational periods:

In order to determine a best fit rotational period, spherical harmonic analyses have been performed on different datasets for both Uranus and Neptune; with the rotational period being treated as a free parameter. The rotational period of both planets has been altered in 1-minute intervals from the currently accepted rotational period, to determine the best fitting rotational period to the representative data.

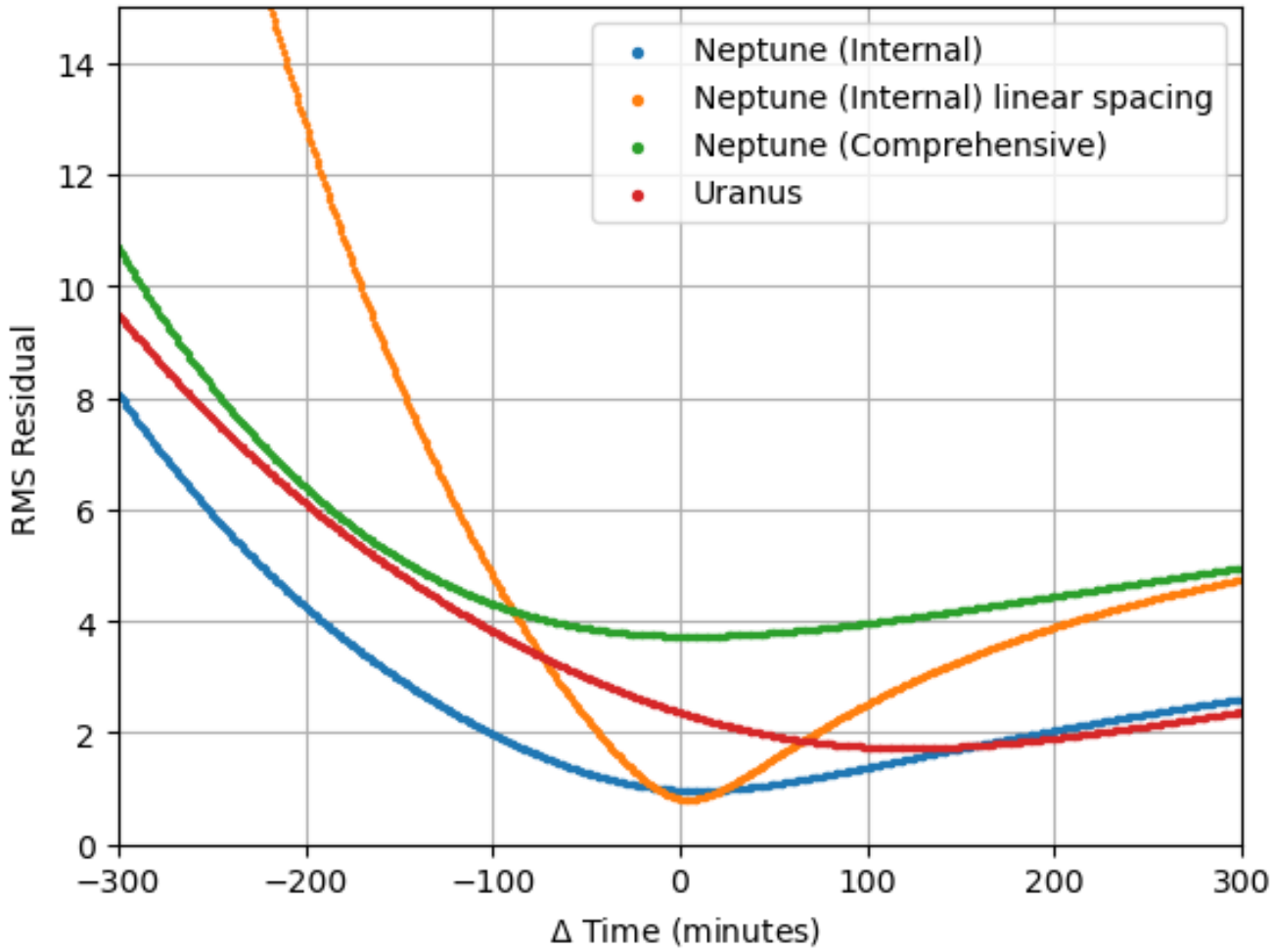

Figure 9: *Misfit to data against change in rotational period for Uranus and Neptune. Neptune's "internal" data refers to the dataset collated by (Connerney et al., 1991), "Comprehensive" is in relation to all of the magnetic data available. All datasets are rejecting all datapoints that are greater than 8 radii away from the planet. The figure has been generated using (Hunter, 2007).*

The minimum for each curve in figure *(9)* represents the rotational period that fits the magnetic data most accurately, it is clear that the rotational period of Neptune is very well constrained. The best-fitting rotational periods are for Neptune: **+10 minutes** for the internal dataset

(Connerney et al., 1991), **+4 Minutes** when assuming a linear spacing between those data, **+6 minutes** for the full Neptune dataset, and for Uranus:**+2 hours and 2 minutes.** Unexpectedly, the linearly (incorrectly) spaced data from Connerney et al. (1991) produces a better-defined minimum, that fits the magnetic data more accurately, and is closer to the currently accepted rotational period of Neptune.

Unless otherwise stated, all field models and results for Neptune will be generated using the data as defined in (Connerney et al., 1991), with the correct spacing between data.

3.2 Choosing appropriate damping parameters:

When trying to constrain a magnetic field model that is both a true representation of the data, and physically plausible – we aim to compromise between the Residual (misfit), by having a model that sufficiently explains all of the data, while still being as smooth (or as simple) as possible. Plotting the Residual (misfit) against the Damping norm (smoothness) for a range of different damping parameters yields a hyperbolic trade-off curve. Examining the trade-off curve, the ideal damping parameter is one at which the model fits the data well, while still being optimally smooth is the "knee"; this is before the value of the damping norm increases exponentially. An "over damped" model would be one formulated with a too high level of damping, with most of the small-scale features removed; whereas an "under-damped" would be a model that is dominated by short wavelength features, increasing the roughness without substantial improvement to the data fit.

3.2.1 Minimising Surface field variation:

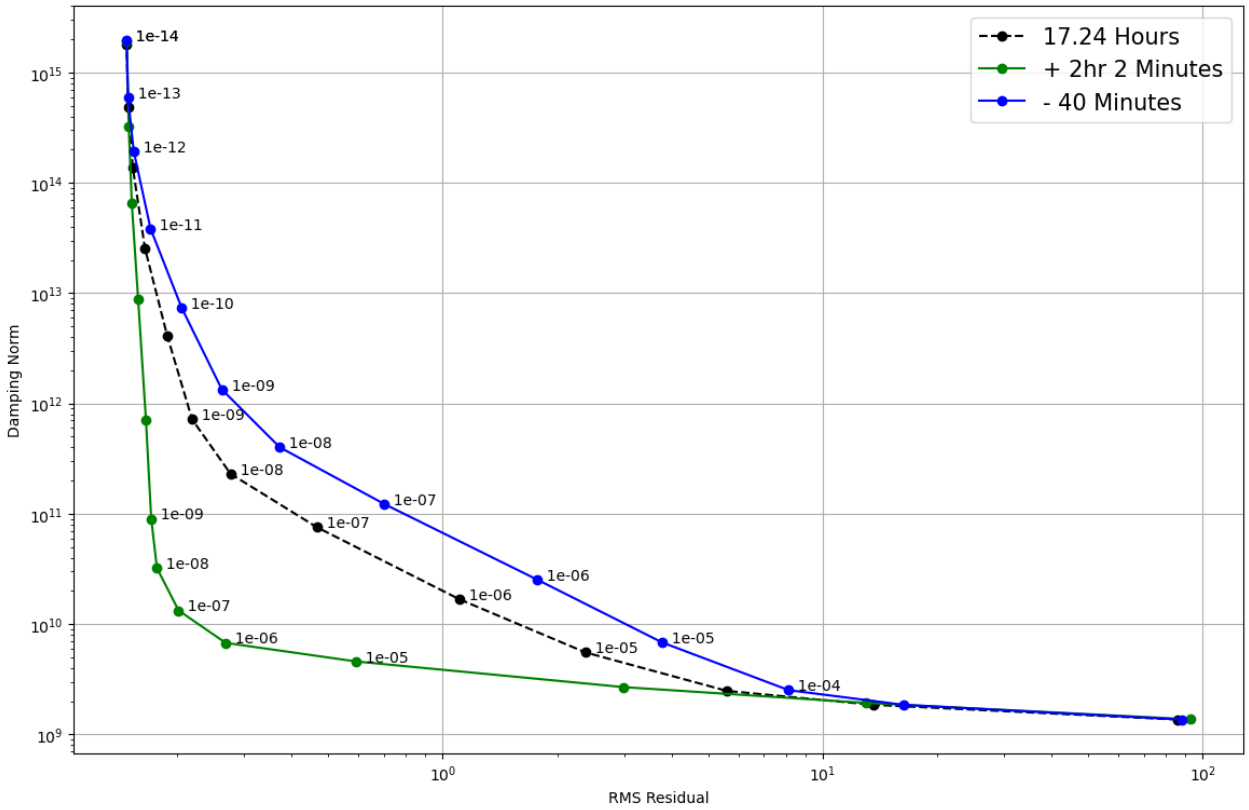

Figure 10: *Trade-off curves for 3 different rotational periods of Uranus. Black – the currently defined rotational period of Uranus, Blue is the rotational period as proposed by Nettelmann et al. (2012), the green line the rotational period suggested by the magnetic data. Figure has been generated by (Hunter, 2007).*

Figure *(10)* shows a clear difference between the different rotational periods that are proposed. The knee of the magnetically suggested rotational period, is much more clearly defined that the other two, and is similarly much closer to the origin. This means that it fits the data significantly more accurately than the other rotational periods, with only a relatively small increase in the complexity of the model, an ideal damping parameter of $\mathbf{1 \times 10^{-7}}$ has been chosen.

However, with the other rotational periods we discover some of the challenges of using this technique to determine magnitude of which to govern the model with damping. The knee of these trade-off curves are not as clearly defined, with the possibility of strong arguments for any damping parameters in the range from: $\mathbf{1 \times 10^{-4}}$ to potentially $\mathbf{1 \times 10^{-8}}$. A damping parameter of $\mathbf{1 \times 10^{-4}}$ for both the currently accepted rotational period, and -40 minutes has

been chosen, as the fit to data is sufficient, all the while not increasing the complexity of the model too drastically compared to previous damping parameters.

The knees in the different trade-off curves for Neptune are significantly clearer than they are for Uranus. From here only the data as defined by Connerney et al. (1991) are going to be used, as seen in figure *(9)* the minimum was more clearly defined than the full Neptune dataset. Due to the proximity of the two curves between the currently accepted rotational period, and that of magnetically suggested data, no annotations of damping parameters have been made on the figure, $\mathbf{1 \times 10^{-7}}$ is the chosen damping parameter of the knee for all rotational periods.

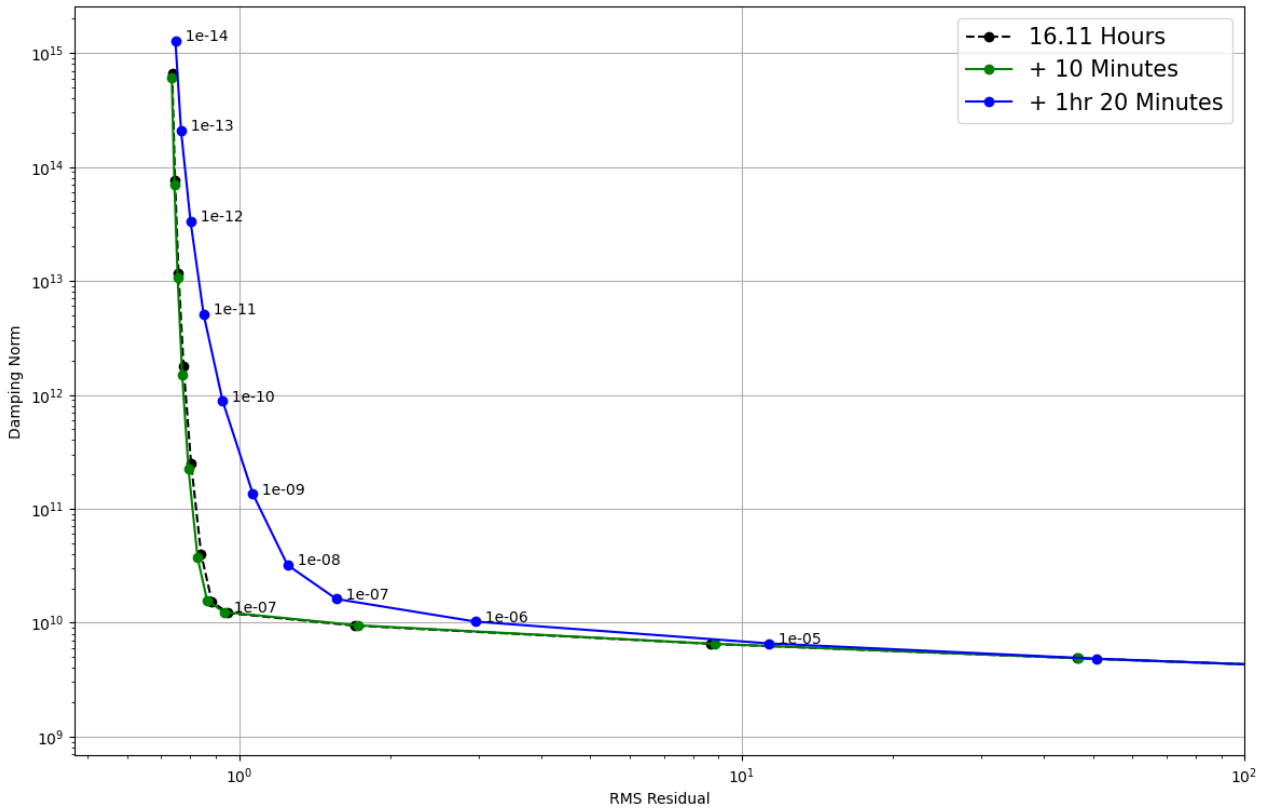

Figure 11: *Trade-off curves for 3 different rotational periods of Neptune. Black – The currently defined rotational period of Uranus, Blue is the rotational period as proposed by (Nettelmann et al., 2012), the green line the rotational period suggested by the magnetic data. Figure has been generated by (Hunter, 2007).*

3.2.2 Minimising the Ohmic heating norm:

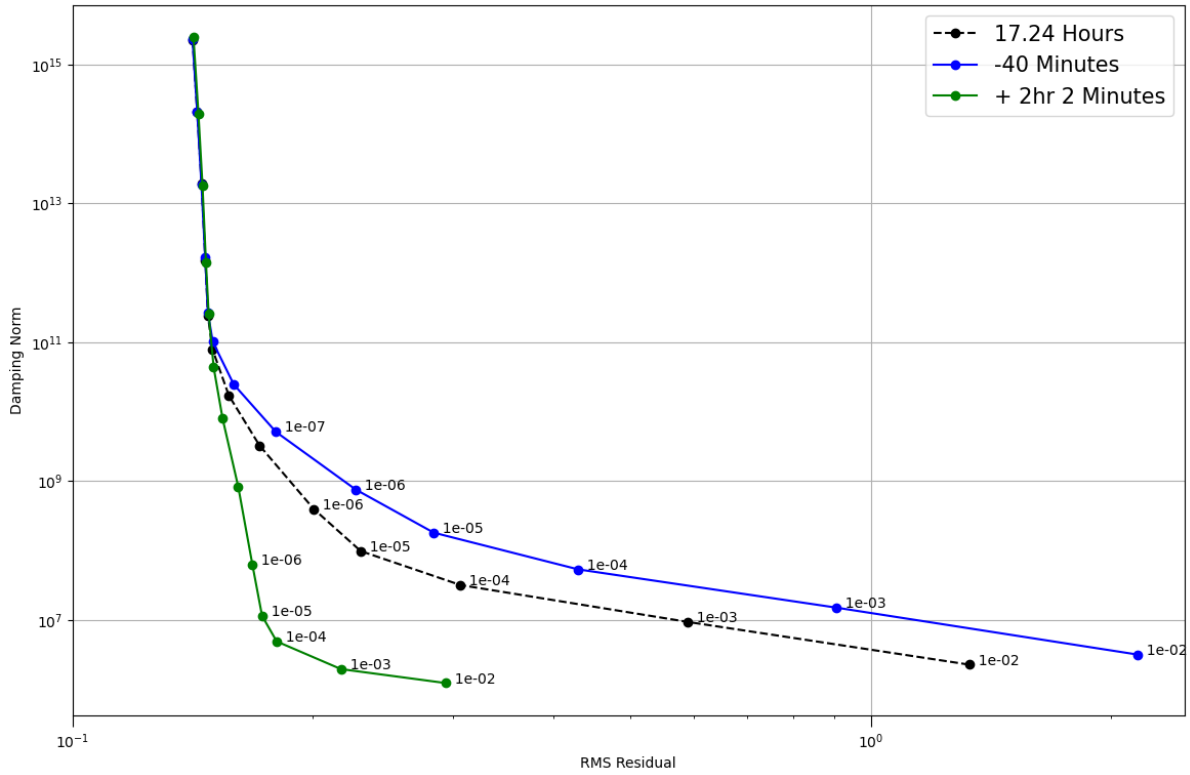

Figure 12: *Trade-off curves for 3 different rotational periods of Uranus, at the depth of the source at $0.75R_U$. Black – The currently defined rotational period of Uranus, Blue is the rotational period as proposed by (Nettelmann et al., 2012), the green line the rotational period suggested by the magnetic data. Figure has been generated by (Hunter, 2007).*

At the depth of $0.75R_U$, the knee from the rotation period suggested by the magnetic data is very similarly defined as to that at the surface, as shown in figure *(12)*. However, the other knees from the two rotational periods are similarly ill defined. An ideal damping parameter of $\mathbf{1 \times 10^{-4}}$ has been chosen for the magnetic data, and $\mathbf{1 \times 10^{-5}}$ for the other two.

Below, in figure *(13)*, at a depth of $0.8R_N$, the ideal damping parameters, found in the knees of the trade-off curves for all datasets are $\mathbf{1 \times 10^{-4}}$.

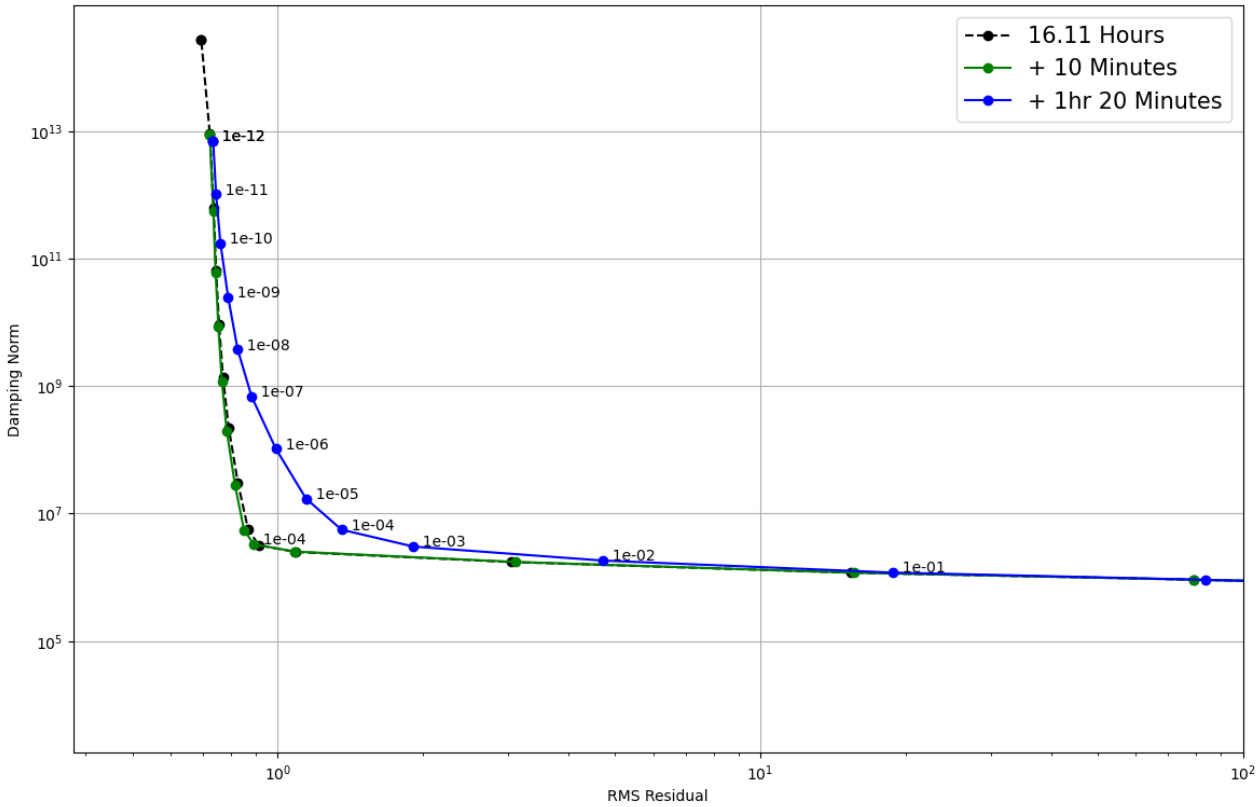

Figure 13: *Trade-off curves for 3 different rotational periods of Neptune, at the depth of the source at $0.8R_N$. Black – The currently defined rotational period of Uranus, Blue is the rotational period as proposed by (Nettelmann et al., 2012), the green line the rotational period suggested by the magnetic data. Figure has been generated by (Hunter, 2007).*

3.3 Magnetic field models:

For each planet, the internal field gauss coefficients are calculated up to degree 16.

When calculating the Neptune – no external field coefficients are calculated, and for Uranus they've only been calculated to degree one.

$$\boldsymbol{NParameters = l_{INT}(l_{INT} + 2) + l_{ext}\,(l_{ext} + 2)} \qquad 22$$

From equation *(22)*, the total number of gauss coefficients calculated for each planet are Neptune: 288, and Uranus: 291.

Here follows a range of different magnetic field models of both planets, for a range of different damping parameters for each of the rotational period estimates.

3.3.1 Currently accepted rotational periods:

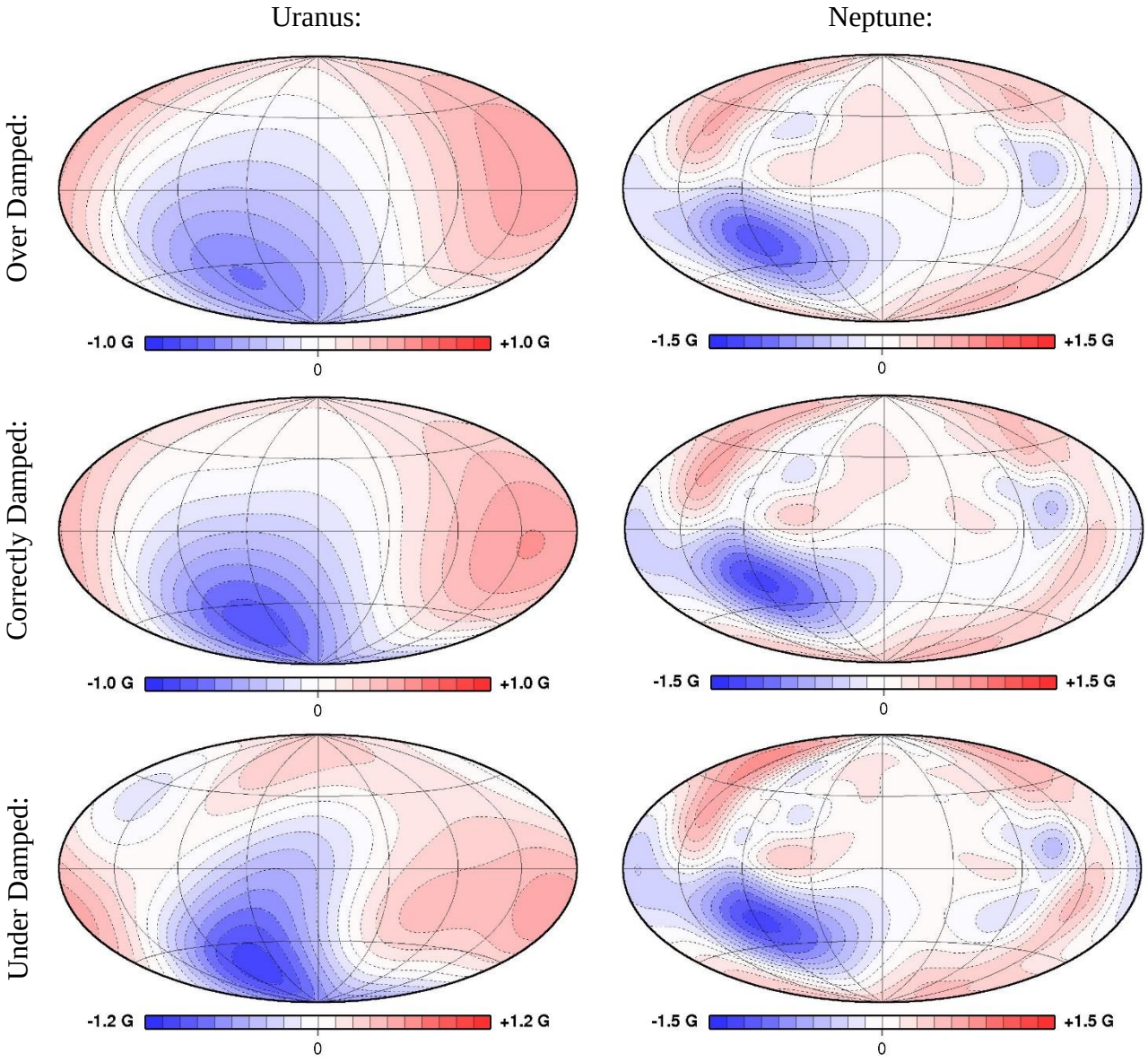

Figure 14: Magnetic field models, B_r for both Uranus and Neptune, with the smoothing surface constraint - at a range of damping parameters. The currently accepted rotational periods are 17.24 and 16.11 hours respectively. For Uranus, the chosen damping parameters are (Top to bottom): $1 \times 10^{-3}, 1 \times 10^{-4}, 1 \times 10^{-5}$. *For Neptune the chosen camping parameters are (Top to Bottom):* $1 \times 10^{-6}, 1 \times 10^{-7}, 1 \times 10^{-8}$. *The colourbar is indicitive of the intensity of the magnetic field, in units of Gauss – 1 G =* $10^5 nT$. *All maps are produduced using GMT Software (Wessel and Smith, 1991) with a Hammer Equal area projection. Here, the west longitude coordinate system of (Connerney et al., 1987, 1991), with zero longitude at the edge of the maps.*

3.3.2 Alternative periods of Uranus:

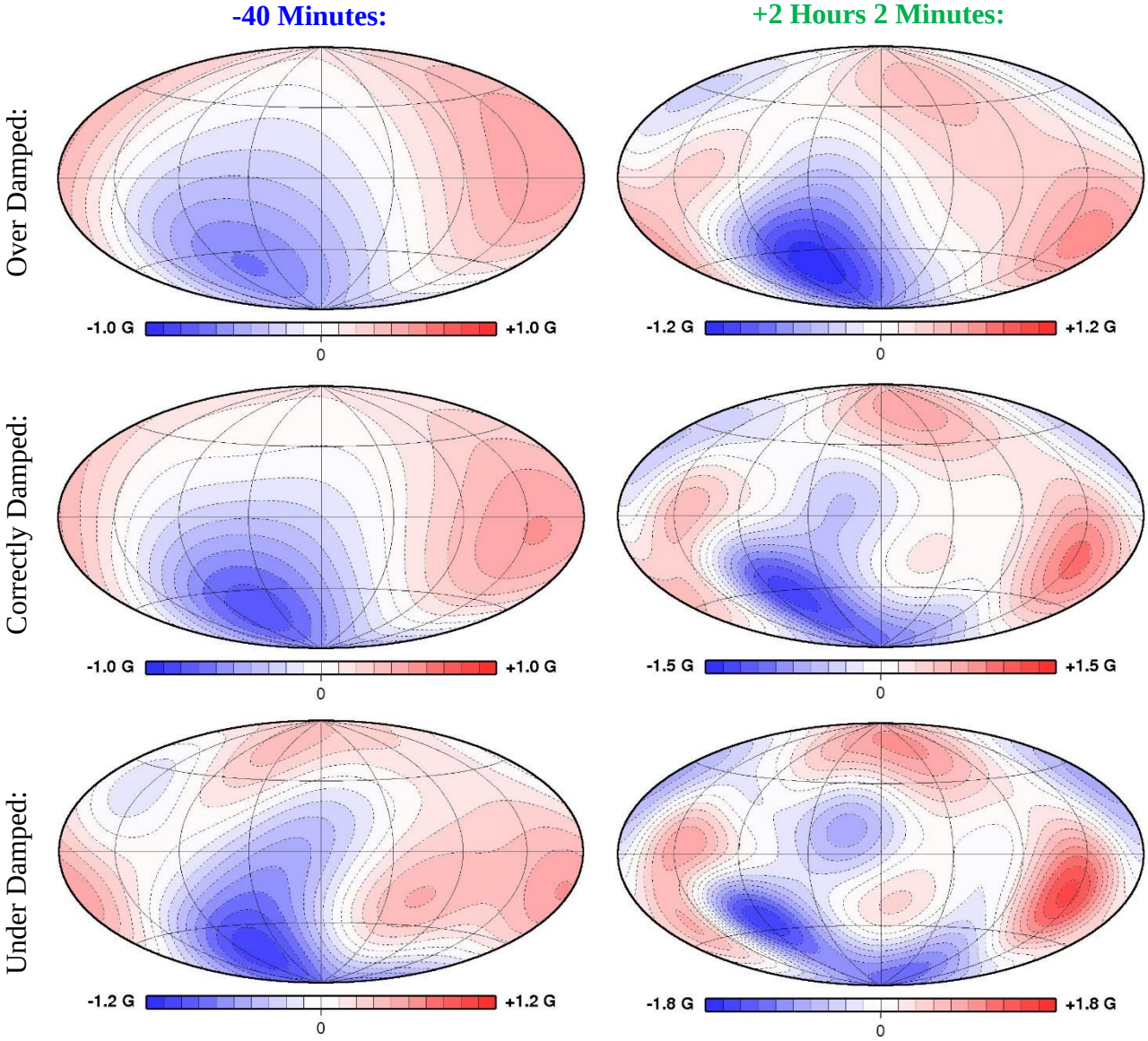

Figure 15: *Magnetic field models, B_r for Uranus, with the smoothing surface constraint - at a range of damping parameters. The currently accepted rotational period is 17.24 Hours.* For -40 minutes, the chosen damping parameters are (Top to bottom): $1 \times 10^{-3}, 1 \times 10^{-4}, 1 \times 10^{-5}$. *For +2 Hours 2 minutes the chosen camping parameters are (Top to Bottom):* $1 \times 10^{-6}, 1 \times 10^{-7}, 1 \times 10^{-8}$. *The colourbar is indicitive of the intensity of the magnetic field, in units of Gauss – 1 G =* $10^5 nT$. *All maps are produduced using GMT Software (Wessel and Smith, 1991) with a Hammer Equal area projection. Here, the west longitude coordinate system of (Connerney et al., 1987, 1991), with zero longitude at the edge of the maps.*

3.3.3 Alternative periods of Neptune:

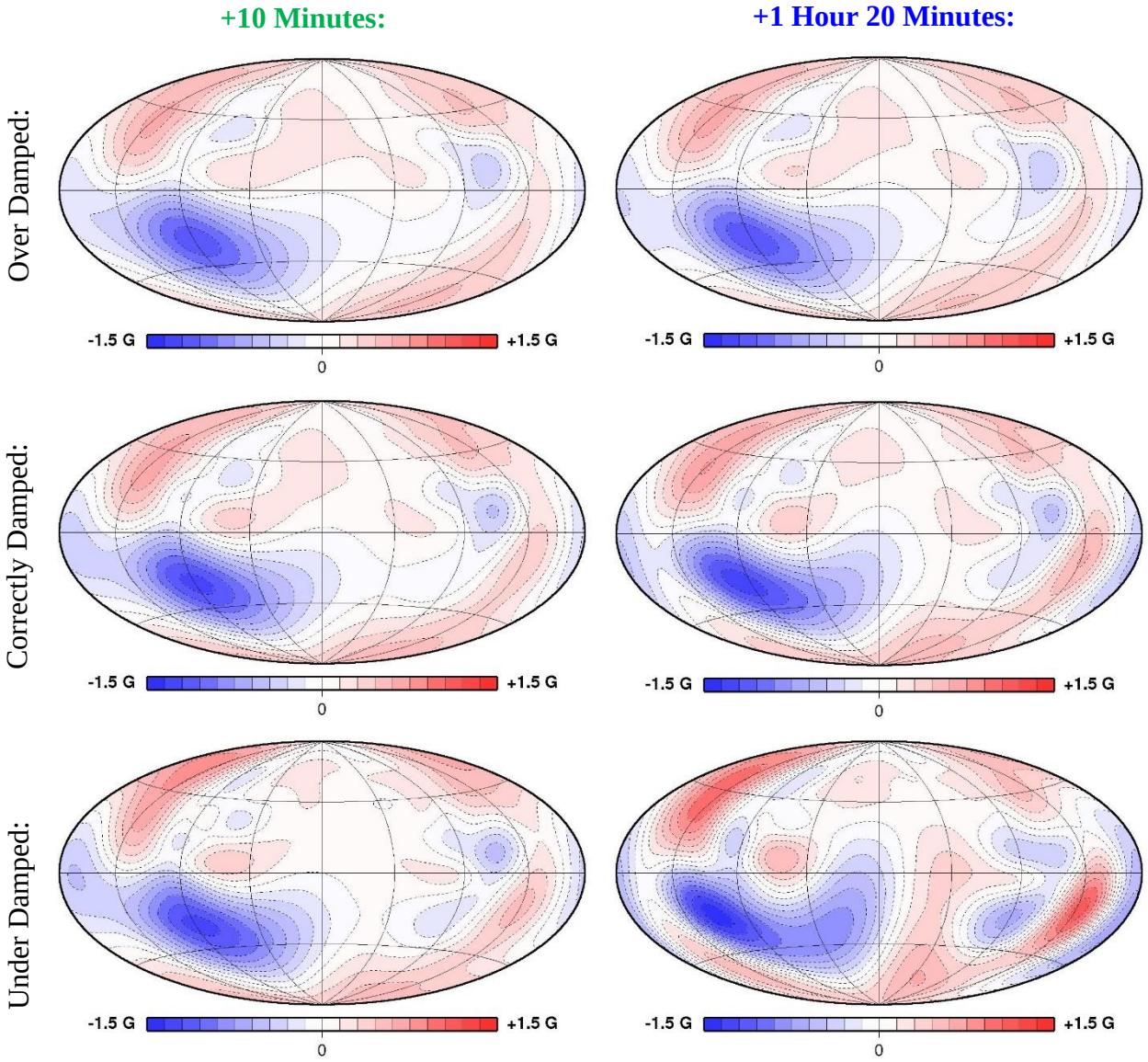

Figure 16: *Magnetic field models, B_r for Neptune, with the smoothing surface constraint - at a range of damping parameters. The currently accepted rotational period is 16.11 Hours.* For +4 minutes, the chosen damping parameters are (Top to bottom): $1 \times 10^{-6}, 1 \times 10^{-7}, 1 \times 10^{-8}$. *For +1 Hour 20 minutes the chosen camping parameters are (Top to Bottom):* $1 \times 10^{-6}, 1 \times 10^{-7}, 1 \times 10^{-8}$. *The colourbar is indicitive of the intensity of the magnetic field, in units of Gauss – 1 G =* 10^5*nT. All maps are produduced using GMT Software (Wessel and Smith, 1991) with a Hammer Equal area projection. Here, the west longitude coordinate system of (Connerney et al., 1987, 1991), with zero longitude at the edge of the maps.*

3.3.4 At the depth of the source:

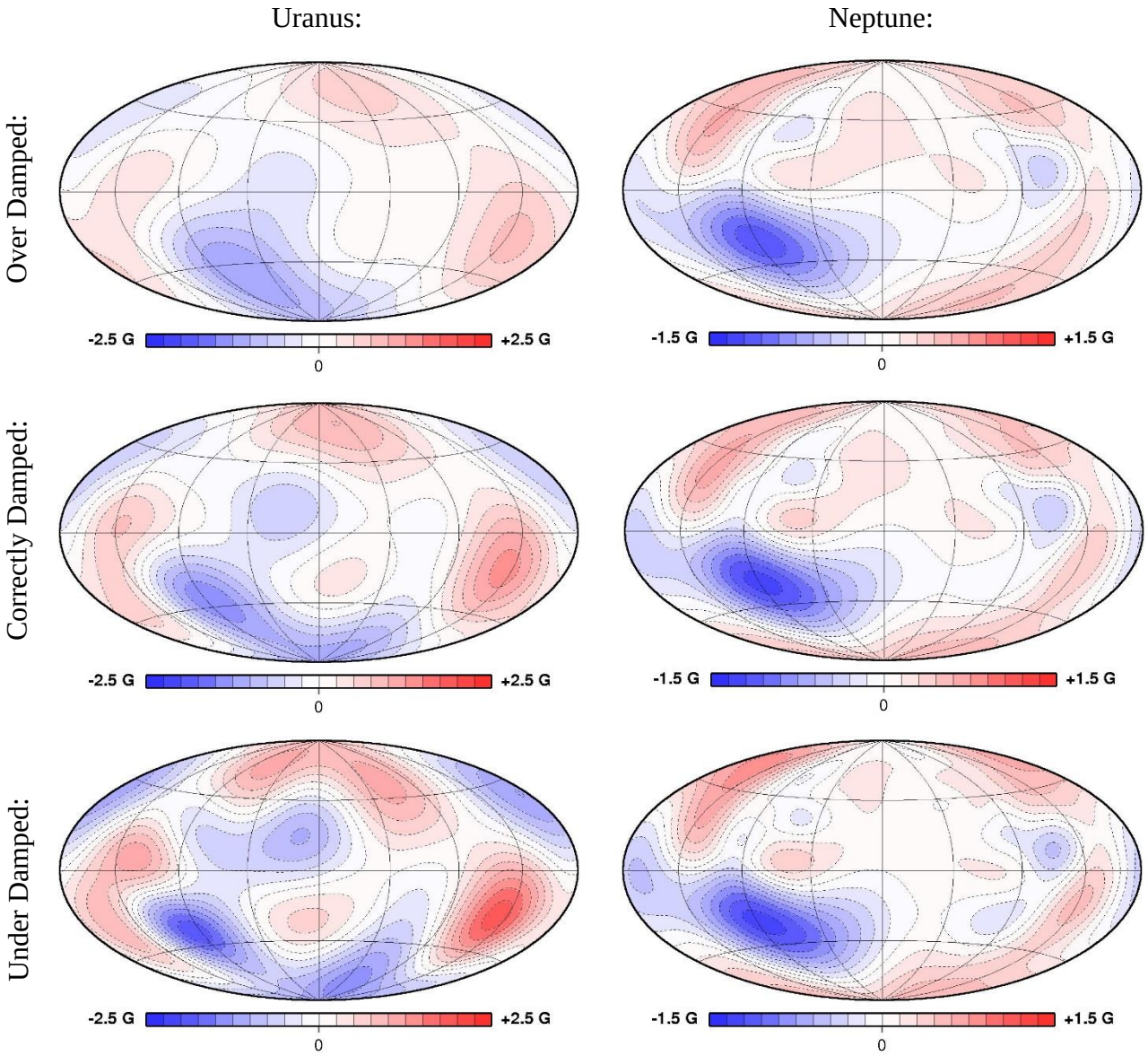

Figure 17: *Magnetic field models, B_r for the best fit rotational periods both Uranus and Neptune (+2hrs 20 minutes, +4 minutes), with the Ohmic Heat constraint applied at $0.75R_U$ and $0.8R_N$ respectively, at a range of damping parameters. The currently accepted rotational periods are 17.24 and 16.11 hours respectively.* For Uranus, the chosen damping parameters are (Top to bottom): $1 \times 10^{-3}, 1 \times 10^{-4}, 1 \times 10^{-5}$. *For Neptune the chosen camping parameters are (Top to Bottom):* $1 \times 10^{-6}, 1 \times 10^{-7}, 1 \times 10^{-8}$. *The colourbar is indicitive of the intensity of the magnetic field, in units of Gauss – 1 G =* 10^5*nT. All maps are produduced using GMT Software (Wessel and Smith, 1991) with a Hammer Equal area projection. Here, the west longitude coordinate system of (Connerney et al., 1987, 1991), with zero longitude at the edge of the maps.*

3.4 Field map differences:

3.4.1 Uranus:

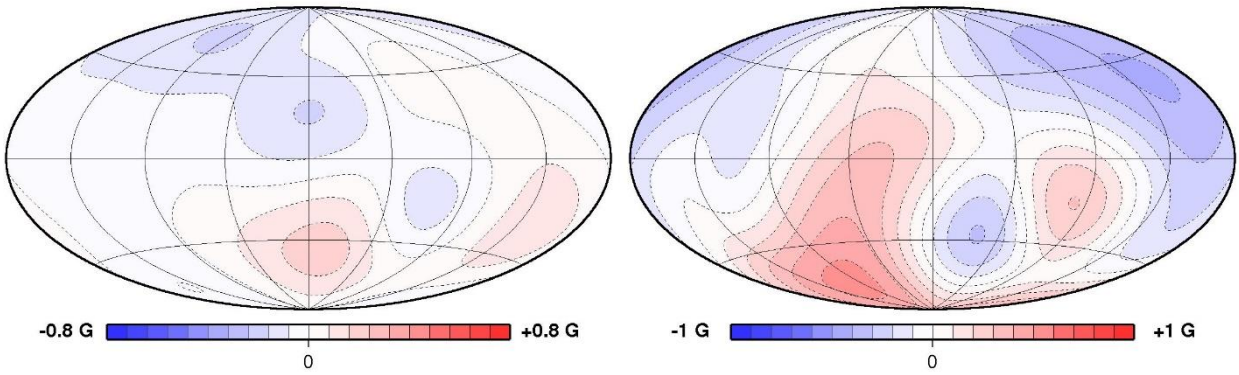

Figure 18: *Field map differences of Uranus, at a constant RMS Residual (Misfit value – 2.37 2dp). LEFT is the difference in field models between the currently accepted rotational period and +40 minutes, RIGHT is the difference in field models between the currently accepted rotational period and +2 hours 2 minutes. The colourbar is indicitive of the intensity of the magnetic field, in units of Gauss – 1 G =* 10^5*nT. All maps are produduced using GMT Software (Wessel and Smith, 1991) with a Hammer Equal area projection. Here, the west longitude coordinate system of (Connerney et al., 1987, 1991), with zero longitude at the edge of the maps.*

3.4.2 Neptune:

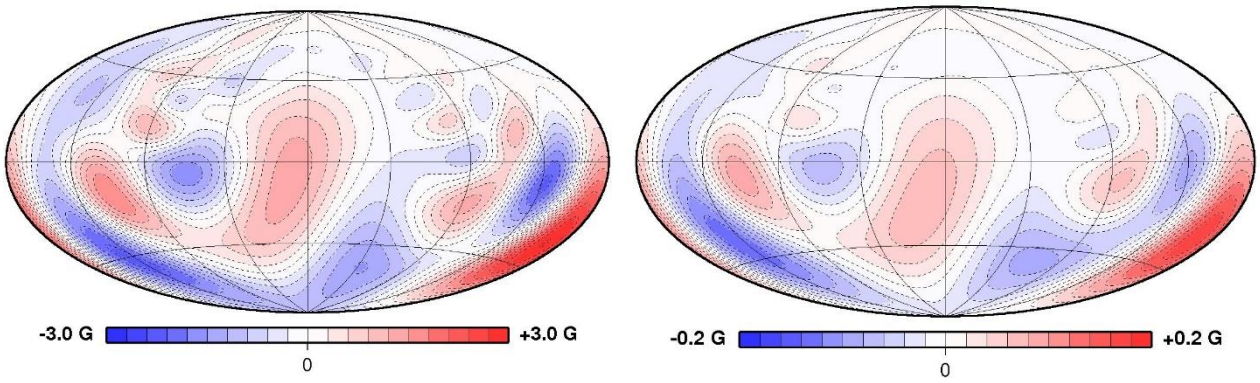

Figure 19: *Field map difference of Neptune, at a constant RMS Residual value (Misfit value – 1.25 2pd). LEFT is the difference in field models between the currently accepted rotational period and +1hr 20 minutes. RIGHT is the difference in field models between the currently accepted rotational period and + 10 minutes. The colourbar is indicitive of the intensity of the magnetic field, in units of Gauss – 1 G =* 10^5*nT. All maps are produduced using GMT Software (Wessel and Smith, 1991) with a Hammer Equal area projection. Here, the west longitude coordinate system of (Connerney et al., 1987, 1991), with zero longitude at the edge of the maps.*

Through figures *(14)*, to *(17)*, a range of different field maps have been produced, initially those of the currently accepted rotational periods, then on to compare the best fit rotational periods of both planets as both suggested from the magnetic data, and that of Nettelmann et al. (2012).

We argue that for both planets, at most of the respective rotational periods, all of the main features are robust, and consistent throughout all models produced, with a range of different damping parameters.

Despite this, there are more noticeable features and structures present within different models – perhaps the most notable being the significant increase in short wavelength structure in the Uranus model, in the rotational period suggested by the magnetic data (green), all the while having a better fit to data. This can be seen from figure *(18)* where the differences plot between the gravitational data and the currently accepted rotation period are more similar than that of the Magnetic data for an equivalent fit to data. This is in contrast to the models generated for Neptune, in figure *(19)* where the rotational period as suggested by the magnetic data matches the currently accepted rotational period much more closely than the data suggested by the gravitational estimates. There is no apparent difference in the field structure between the two, with the main difference being in amplitude. For that produced from the gravitational data (Nettelmann et al., 2012), there is some change in the short wavelength features, introducing short wavelength features in the northern hemisphere that aren't present In the other field models.

3.5 Power Spectra Analysis:

Leading from the different spherical field models that we have obtained; we follow by investigating the contribution of each spherical harmonic degree to the total field intensity. The power spectrum has been computed at both the surface of each planet, and then down at the depth of field generation $0.75R_U$ and $0.8R_N$ for Uranus and Neptune respectively (Holme and Bloxham, 1996).

Figure *(20)*, shows the power spectrum normalised at the surface with the smoothing constraint applied for both Uranus and Neptune, following in figure *(21)*, the power spectra for the best fit rotational periods of each planet are plotted at $0.75R_U$and $0.85R_N$ respectively.

3.5.1 Minimising Surface field variation:

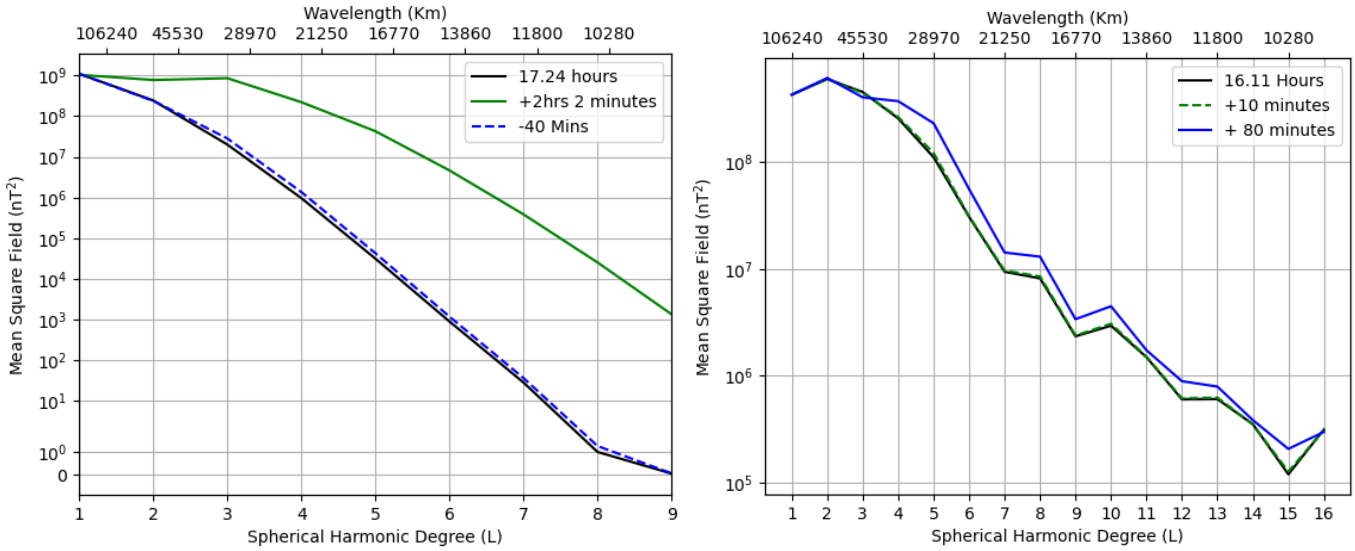

Figure 20: *Power Spectrum of both Uranus (Left) and Neptunes (Right) magnetic field at the surface of the planet for the ideal damping parameter, employing the smoothing norm. Figures have been created using (Hunter, 2007).*

One of the most striking differences between the different rotational periods, is the relative increase contribution from almost every harmonic degree to the mean square field of Uranus for the rotational period suggested by the magnetic data.

This is a direct reflection of the magnetic field models, where there is significantly higher contribution to short wavelength features; this increase in higher degree harmonic signal will be predominantly caused by the smaller damping parameter chosen, allowing for more short wavelength features to be present in the field model. The other rotational periods are almost identical in terms of harmonic degree – the field models of Uranus have traditionally been very simple, for example see: (Connerney, 1993; Holme and Bloxham, 1996); with by far the largest contributions to the field being degree 1, primarily an offset dipolar field. From section 2.4, we can further see that there the signal whitens at approximately degree 8 or degree 12 for the rotational period suggested by the magnetic data, equivalent to the source of the field being at approximately 0.75 R_U, consistent with Holme and Bloxham (1996) or 0.5 R_U respectively.

For all rotational periods of Neptune, the main contribution to the geomagnetic field is that of degree 2, with the currently accepted rotational period, and that suggested by the magnetic data being almost identical – with some slight deviations at higher degrees. The field composition as suggested by Nettelmann et al. (2012), is significantly different, with a larger field contribution at all higher degrees than the other models.

3.5.2 Minimising the Ohmic heating norm:

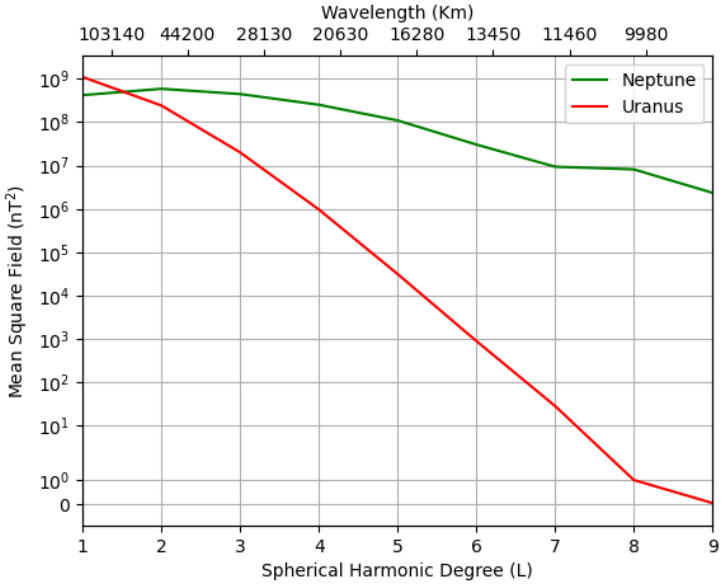

Figure 21: *Power Spectrum of best fit rotational periods of both planets, with the Ohmic heating norm applied at $0.75R_U$ and $0.8R_N$ with the ideal damping parameter of 1×10^{-4}each. Figure generated using (Hunter, 2007).*

The structure of the fields at depth are very similar to that at the surface, with a stronger field intensity being found at the depth of source generation, with the prevailing field structure and components being of similar proportions.

3.6 Error Analysis:

We can plot the misfit to the data against time, shown in figure *(22)* and *(23)* for Uranus and Neptune respectively.

There is a really sharp reduction in the misfit to the Uranus data for the rotational period suggested by the gravitational data – there is an almost complete reduction in the error in each orthogonal component, with the largest remaining error in the X-component. Section 2.5 has already elaborated on this, but the sharp spikes in the data at approximately 40000 seconds are a function of spacecraft attitude. (Connerney et al., 1991, 1987) explain that the attitude was generally within 0.05° for Uranus, and up to 0.1° for the Neptune encounter – making the source of error comparable to that of instrument sensitivity (Holme and Bloxham, 1996). Where the sources of error are much greater, only the measurements of total field intensity should be used – with more explanation for modelling attitude error found in Holme and Bloxham (1995).

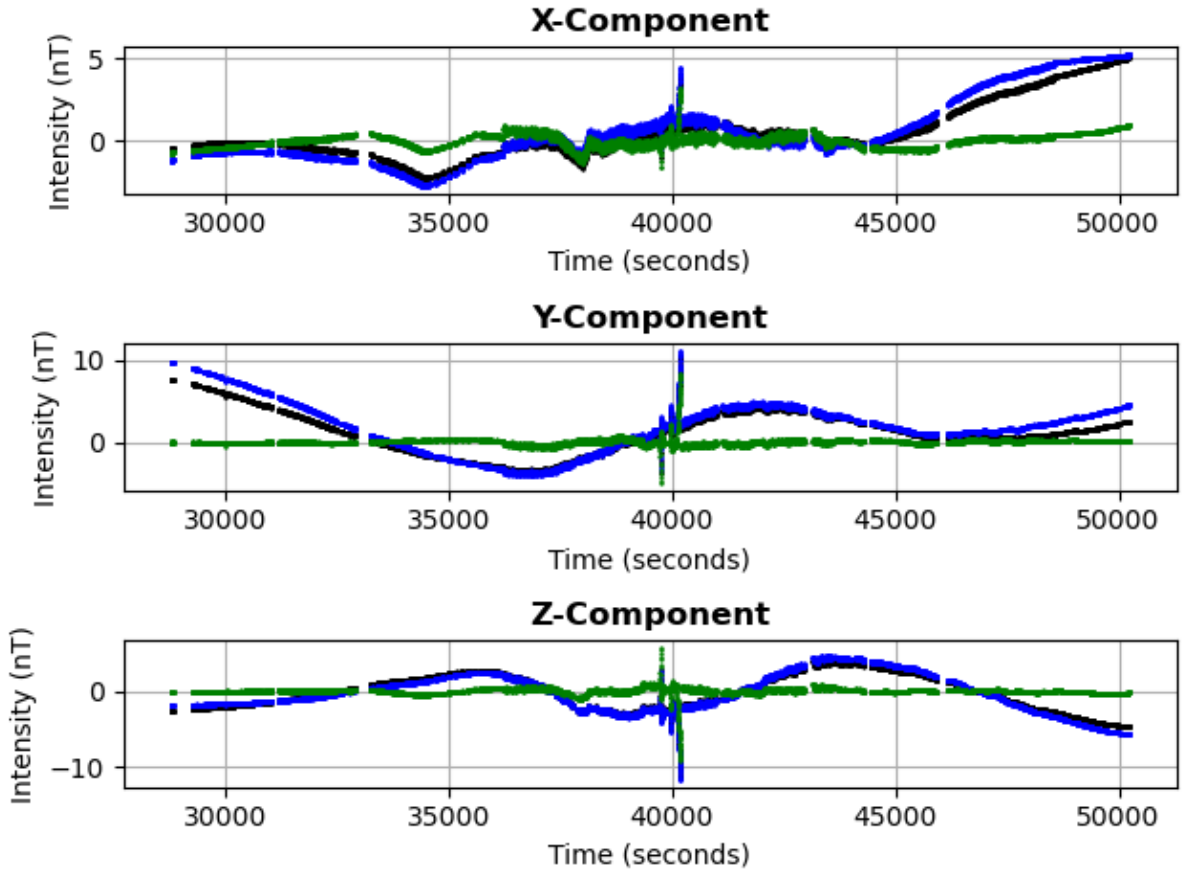

Figure 22: *The misfit of the data to the model for each orthogonal magnetic component of Uranus. Black: Currently accepted rotational period (17.24 Hours), Blue: as suggested by the Gravitational data (- 40 minutes). Green: as suggested by the magnetic data (+ 2 Hours and 2 minutes). The x-axis is time in seconds, measured from the start of the Voyager 2 encounter. Figure created using (Hunter, 2007).*

The rotational period as suggested by Nettelmann et al. (2012) also appears to fit the data consistently worse throughout the entire encounter – with everything being best defined near closest approach for the encounter. There is also what appears to be a harmonic signal present through the other components, over an approximate 40,000 second period – most notably through the Y-Component.

Holme and Bloxham, (1996) suggest that the field components vary smoothly in the planetocentric reference frame because of the smooth rotation of the spacecraft with respect to the planetocentric frame. When modelling a geomagnetic field, uncorrelated errors are necessary to produce models that are independent of each other, and do not contain any form of systematic bias in the estimation of the field parameters; from figure *(22)* the harmonic signal present for two of the datasets shows a clear correlation between data. This correlation could be due to every other parameter other than longitude being equivalent; al field components have been measured at similar places in space at the same time, local correlation can be allowed for easily, and at no extra numerical cost (Holme, 2000).

While there is also some structure present in the misfit of Neptune – the results appear to be much less correlated and structured. Figure *(23)* shows the error of the data when correctly spaced, with more data about closest approach; figure *(24)* shows the error on the data when there is an assumed linear spacing between them. The stretching present on the x-axis between figures *(23)* and *(24)* is due to the difference in assumed time between the data; but the overall structure of the errors is incredibly similar: with the model as suggested by the gravitational rotational period fitting the data the least, and the model as suggested by the magnetic data fitting the best. The most notable difference between the two is the general reduction of the error throughout the series, from the data with the correct time spacing. There are also significantly more random errors about closest approach for both datasets, with the smallest recorded errors present when sampling using the LFM range 5. While these errors appear large it is worth acknowledging that they are very small, in relation to the total intensity of the magnetic fields or Uranus and Neptune (413 nT and 9950 nT respectively).

Overleaf, figure *(25)* show a potential correlation between the misfit to data for different rotational periods of Uranus, where the magnitude of each component has been scaled artificially to make them of comparable magnitude.
For no change in the rotation period, there is some correlation between the misfit to data, and the first derivative of the magnetic data. This correlation is likely to be caused by some inconsistency in the times at which data is recorded, potentially because of a lag between the recorded time of data acquisition, and the true time of acquisition.

For the magnetically derived rotational period, the misfit to data and the derivative of the data appear almost inversely correlated. With certainly no immediate links between the two sets of data, suggesting that the rotational period as suggested by the magnetic data does not have to the same degree an inconsistency with the time of recorded data.

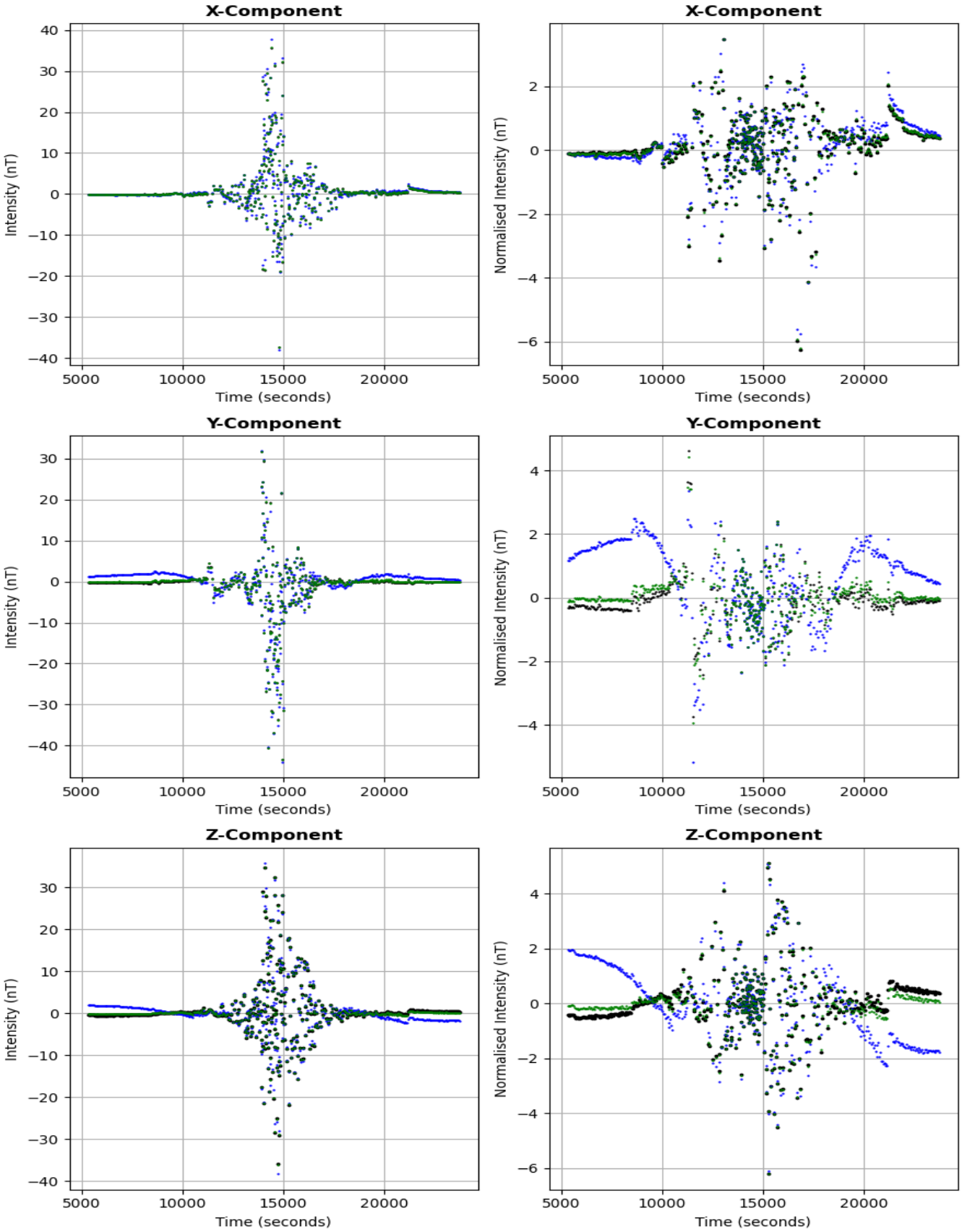

Figure 23: *The misfit of the model to the data for each orthogonal magnetic component of Neptune. Black: Currently accepted rotational period (16.11 Hours), Blue: as suggested by the Gravitational data (+ 1 hour 20 minutes). Green: as suggested by the magnetic data (+ 10 minutes). Left hand column is the misfit to data, right hand column is the misfit normalised by the error on the data. Figure created using (Hunter, 2007).*

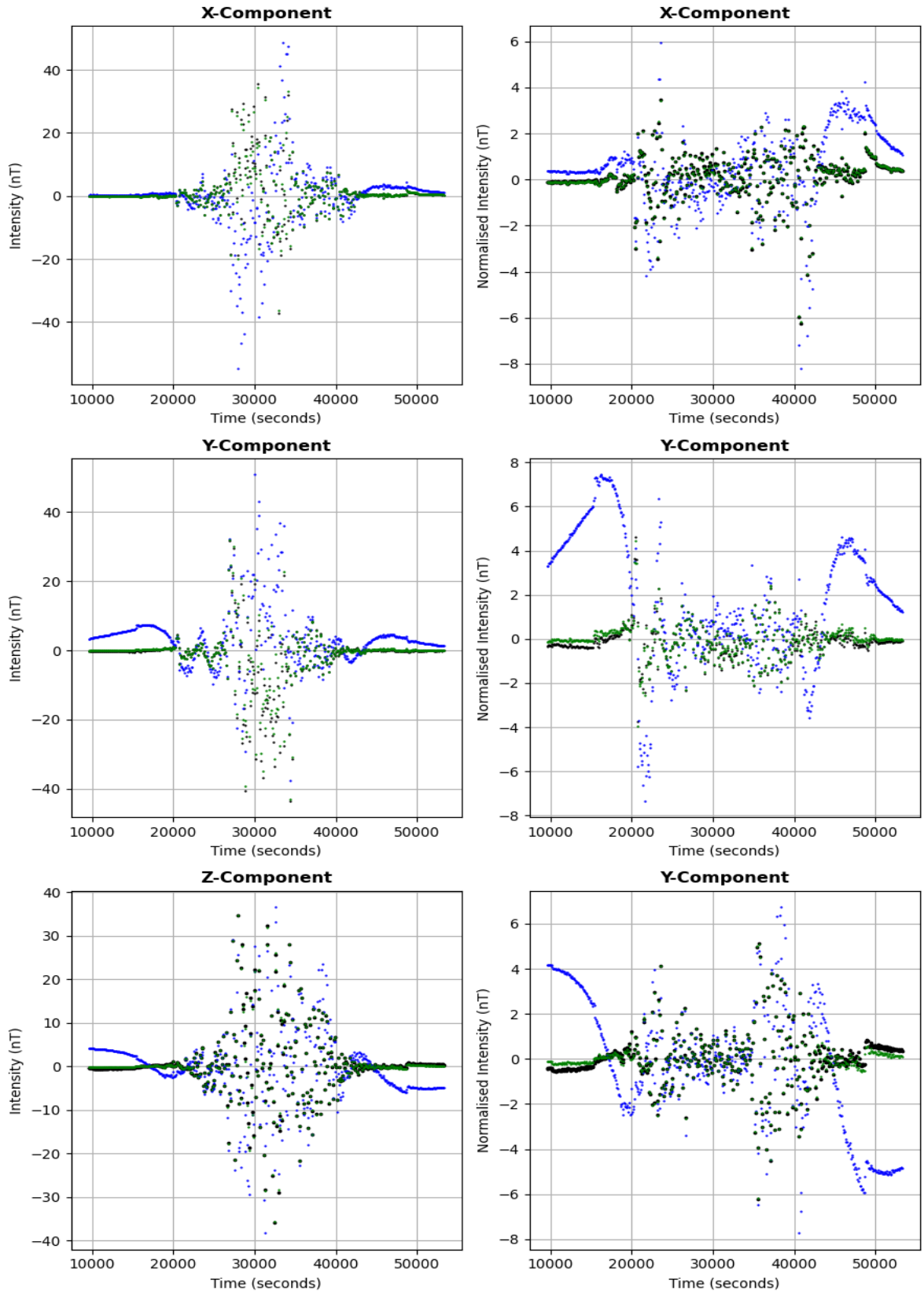

Figure 24: *The misfit of the model to the data for each orthogonal magnetic component of Neptune, When assuming a linear spacing between data. Black: Currently accepted rotational period (16.11 Hours), Blue: as suggested by the Gravitational data (+ 1 hour 20 minutes). Green: as suggested by the magnetic data (+ 4 minutes). Left hand column is the misfit to data, right hand column is the misfit normalised by the error on the data. Figure created using (Hunter, 2007).*

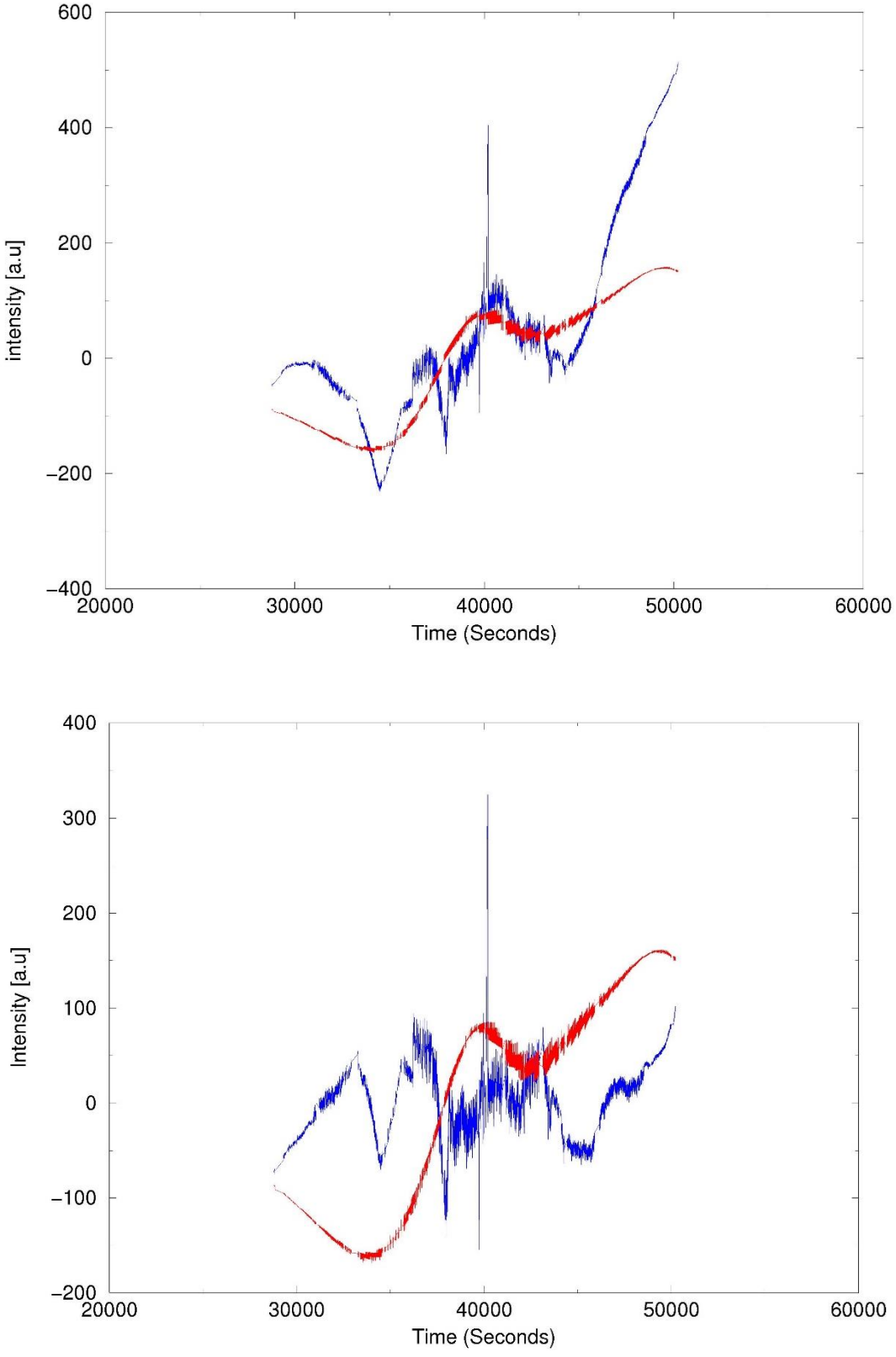

Figure 25: *Examples of correlated (Top) and non-correlated data (Bottom) for the rotational periods of Uranus of 17.24 Hours, and +2Hr 2 Mins respectively. Blue: Scaled misfit to data, Red: Scaled forward difference of the magnetic data. Figure has been generated using GMT Software (Wessel and Smith, 1991).*

3.7 Why are there differences in rotation estimates?

Through the construction of different magnetic models, either from derived gravity observations, or in best fit geomagnetic observations, we are constantly plagued by non-uniqueness.

Through Voyager 2's singular flypast of both Uranus and Neptune, there is only a finite amount of data available to try and model very complex planetary systems. These systems have millions of unknown variables and parameters, causing there to be a range of different ways of constructing models to satisfy all of the known data.

Comparing the results found in these thesis to the results found by Nettelmann et al. (2012), highlight the dangers of non-uniqueness.

Solutions for the best fit rotational period of both planets are found, that satisfy all of the available data in each instance, but our findings are not in agreement. We find it plausible therefore that Nettelmann et al. (2012) make underlying assumptions that govern their gravitational models, altering the predicted rotation period of the planets, including:

- Both Uranus and Neptune have an adiabatic temperature gradient, whereas other sources, such as: (Helled et al., 2010; Helled and Fortney, 2020) argue that Uranus may not. This leads to discrepancies in composition the interior structure of the planet, along with a different planetary model structures being less homogeneous.
- They assume a constant He:H mass ratio at different depths in specific envelopes – leading for the possibility of a different internal structure than expected.
- An iterative scheme has been used to fit the model parameters: (element mass fractions in the inner and outer envelopes Z2 and Z1), the mass of the core, and possible transition pressure between the said envelopes.

  Their scheme fits the gravitational coefficients and the condition of mass conservation; however, it is possible that that the iterative scheme may converge to multiple different solutions that all satisfy the fitting criteria, not just the one they have selected.
- Models for the cooling times of the planets also neglect the presence of clouds and hazes – though to be present in the troposphere (Gautier et al., 1995). Therefore, the full uncertainty on the cooling time is not known. They also neglect the time-dependence of the thermal radiation of the rotation rate due to angular momentum conservation, and of the energy of the rotation.

While this list is not exhaustive, these are all possible sources of non-uniqueness when deriving rotation periods for the planets, and possible causes of the difference in period when compared to this thesis.

Many of the physical properties of the outer planets still remain elusive to us, and to this day the only in-situ measurements we have of the planets are those acquired by Voyager; therefore, it is important to make the distinction between models that fit the data that we have direct measurements of, and models that fit assumed knowledge of the planets and their composition.

3.8 Discrepancies between datasets for Uranus:

The claimed rotational period of Uranus is 17.24 Hours, as defined by Desch et al. (1986) who employed a very similar approach to work done in this thesis, by calculating the RMS Residual error for varying rotational periods, with data within $8R_U$ (dipole filed plus quadrupole internal field plus uniform external field). This data is collated on NASAs PDS website (Lepping, 1993). This data can be seen in figure *(25)* – along with the best fit rotational as derived in this thesis, and the rotational period as used by: Holme and Bloxham, (1996), data analysis done in 1991.

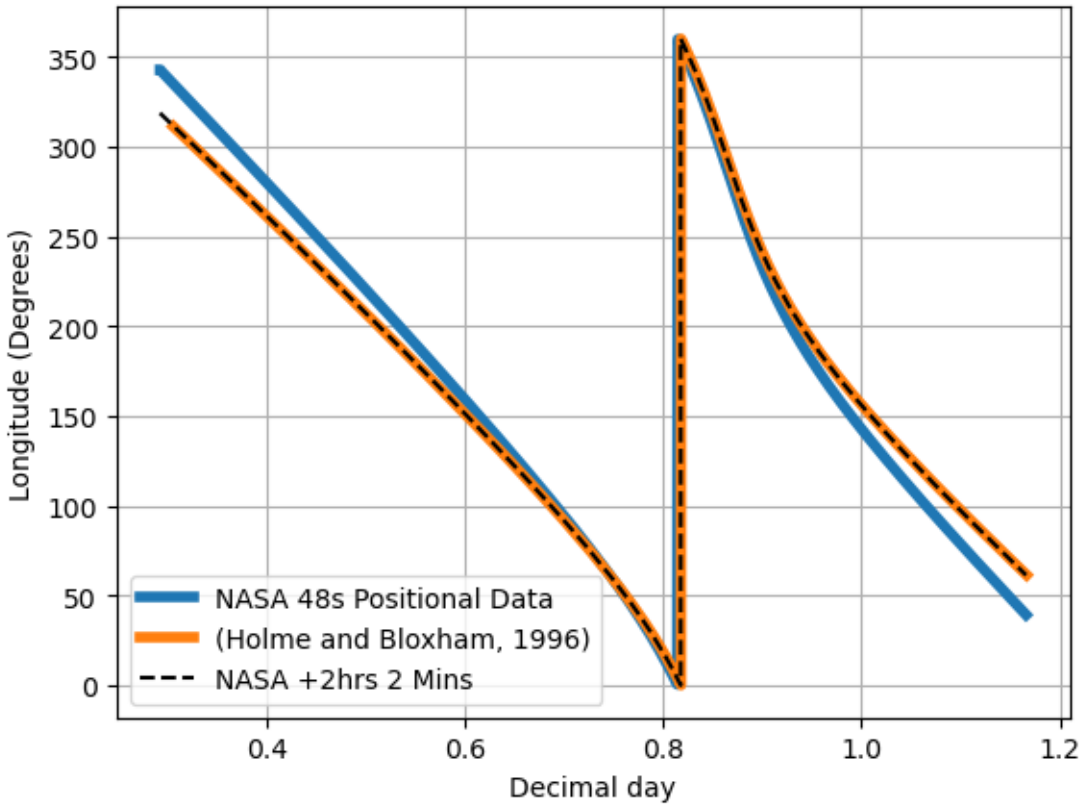

Figure 26: *Rate of Change of Longitude for different datasets of Uranus. Figure has been created using (Hunter, 2007).*

The best fit data as defined in this thesis, and the data used by Holme and Bloxham (1996) are in agreement, but neither agree with Lepping (1993).

There could be several reasons for these differences, a possible explanation being that in 1993, when the dataset used in this thesis was constructed, there could have been an error in either the values of Longitude selected, or in the construction of these values as they are a convolution between Spacecraft Velocity and Planetary rotation rate.
This however does not explain the difference in field composition between the best fit field of Uranus in this thesis; figure *(20),* and that found by Holme and Bloxham (1996). As derived in this thesis, the largest contributor to the mean square field is that of spherical harmonic degree 3, disagreeing with Holme and Bloxham (1996, p16), where degree 1 is the largest contributor.

Chapter 4 - Summary:

In this thesis, we have produced and examined a range of new magnetic field models for Uranus and Neptune, with data obtained by Voyager 2 from inside of 8 radii of the planets. The range of Longitude values as provided by the Nasa planetary data system for the two planets have been synthetically altered from the periods of 17.24 and 16.11 hours respectively. This is so they align with the best fit rotational period as defined by Nettelmann et al. (2012), and the magnetic data themselves. Issues with different datasets for Uranus have been identified, and a possible reason why has been outlined. All of the positional data for Uranus has had a Spline curve ran through the data, to both smooth the data, and allow interpolation to temporal resolution 25x greater than what was acquired. The models have been regularised by a smoothing constraint on the planetary surface, and a lower ohmic heating constraint at the predicted depth of the source of the field. If we under damp all of the field models, they become saturated with short wavelength structure, but fit the data to a higher degree of accuracy; whereas over damped models are much smoother in structure but have an equal increase in the misfit to the data.

The different field models fit the data to different degrees of accuracy, most notably for Uranus; where the rotational period as suggested by the magnetic data generates more field structure than has been previously resolvable, has a lower misfit to the data, and the trade-off curve that it generates over a range of different damping parameters has a much more distinct curve than the other two rotational periods.

For Neptune, the rotational period as suggested by the magnetic data generates a slight improvement to the fit to data, but there is no significant difference in field structure, suggesting the rotational period of Neptune is very well constrained. Therefore the period as suggested by Nettelmann et al. (2012) doesn't appear plausible; as even for the ideally damped model, it simultaneously worsens the fit to the data, and introduces field structure that isn't present in the other models.

The misfit to data for each rotational period has been plotted as a function of time, where the magnetic rotational periods consistently have the lowest misfit, the gravitational predictions consistently the highest misfit – and the currently accepted rotational periods are between the two. The sharp spikes in the misfit data, and that of each orthogonal component of the magnetic field have been identified to be caused by errors with spacecraft attitude, rather than with the magnetometers themselves.

Chapter 5 - Future Work:

One of the main focuses of further work would be the clarification of some discrepancies regarding the rotational period of Uranus.

Trying to decipher the rationale behind decisions that were made in excess of 30 years ago is never going to be easy, but it would be worth investing more effort into trying to uncover why there are differences between different datasets for Uranus. Such as why work done in this thesis, and work by Holme and Bloxham (1996) agree with the rotational period of Uranus, but not with spherical harmonic contributions to the mean field composition, and that neither of our work agrees with the rotation period provided on the PDS website (Lepping, 1993).

Given more time, exploration about the harmonic signal found within the misfits, and the misfits themselves would also be advantageous.

The harmonic signal is notable for both Uranus and Neptune, and analysis should be done further than referencing work that has been done previously. In this thesis, all errors on the results have been treated as uncorrelated, but the harmonic signal present in the misfit to data shows that the errors are correlated. The attitude error, most notably present with Voyager 2's encounter with Uranus should also be corrected for in order to gain a more accurate fit to data than has been achieved in this thesis.

More work could also be done trying to research the apparent correlation between the first derivative of the magnetic data, and the misfit to the data for certain rotational periods. If this is robust, and repeatable for different datasets, it would be worth investing what could be causing this, such as an offset in timing. The degree of correlation between the two values could be calculated to try and determine which rotational periods show the least correlation.

There is another constraint on the field, that due to a lack of time, hasn't been considered. This constraint is the structure of the aurora (Herbert, 2009).

Unfortunately, the data from this study are not available due to the very sad passing of the author in 2010, but the paper presents field maps of auroral intensity and structure. Future work would involve defining a particle tracker, to follow magnetic field lines in produced magnetic field models. We would do this to investigate the influence of different field models on the aurora, in particular looking for models that have possible field spectra but can also reproduce the observed auroral structure.

Acknowledgements:

Initially, I must say a huge thank you must go to my dissertation supervisor, Professor Richard Holme, for his continued support, patience, and care he has provided going far beyond anything that could have been expected from him in my three years at the University of Liverpool.

A thank you must also go to both Charlie and Jack, who make up the rest of our research group. Collectively we have spent a huge amount of time together, working on problems that have affected each of us, the time spent in the Gilbert would have been considerably less bearable without your company!

Finally, thank you Mum.
Thank you for always supporting me, helping me, and pushing me to do things I didn't believe I was capable of doing.

The world is a whole lot emptier without you.

Bibliography:

Behannon, K.W., Acuna, M.H., Burlaga, L.F., Lepping, R.P., Ness, N.F., Neubauer, F.M., 1977. Magnetic field experiment for Voyagers 1 and 2. Space Sci Rev 21, 235–257. https://doi.org/10.1007/BF00211541

Connerney, J.E.P., 1993. Magnetic Fields of the Outer Planets. Journal of Geophysical Research: Planets 98, 18659–18679. https://doi.org/10.1029/93JE00980

Connerney, J.E.P., Acuña, M.H., Ness, N.F., 1991. The magnetic field of Neptune. Journal of Geophysical Research: Space Physics 96, 19023–19042. https://doi.org/10.1029/91JA01165

Connerney, J.E.P., Acuña, M.H., Ness, N.F., 1987. The magnetic field of Uranus. Journal of Geophysical Research: Space Physics 92, 15329–15336. https://doi.org/10.1029/JA092iA13p15329

Constable, C., Parker, R., 1991. Deconvolution of long-core palaeomagnetic measurements?spline therapy for the linear problem. Geophys J Int 104, 453–468. https://doi.org/10.1111/j.1365-246X.1991.tb05693.x

Constable, C.G., Parker, R.L., 1988. Smoothing, splines and smoothing splines; Their application in geomagnetism. Journal of Computational Physics 78, 493–508. https://doi.org/10.1016/0021-9991(88)90062-9

Desch, M.D., Connerney, J.E.P., Kaiser, M.L., 1986. The rotation period of Uranus. Nature 322, 42–43. https://doi.org/10.1038/322042a0

Desch, M.D., Kaiser, M.L., Zarka, P., Lecacheux, A., Leblanc, Y., Aubier, M., Ortega-Molina, A., 1991. Uranus as a radio source., Uranus.

Gautier, D., Conrath, B.J., Owen, T., de Pater, I., Atreya, S.K., 1995. The troposphere of Neptune., Neptune and Triton. ed. University of Arizona Press.

Gurnett, D.A., Kurth, W.S., Poynter, R.L., Granroth, L.J., Cairns, I.H., Macek, W.M., Moses, S.L., Coroniti, F.V., Kennel, C.F., Barbosa, D.D., 1989. First Plasma Wave Observations at Neptune. Science 246, 1494–1498. https://doi.org/10.1126/science.246.4936.1494

Helled, R., Anderson, J.D., Podolak, M., Schubert, G., 2010. INTERIOR MODELS OF URANUS AND NEPTUNE. ApJ 726, 15. https://doi.org/10.1088/0004-637X/726/1/15

Helled, R., Fortney, J.J., 2020. The interiors of Uranus and Neptune: current understanding and open questions. Philosophical Transactions of the Royal Society A: Mathematical, Physical and Engineering Sciences 378, 20190474. https://doi.org/10.1098/rsta.2019.0474

Herbert, F., 2009. Aurora and magnetic field of Uranus. Journal of Geophysical Research: Space Physics 114. https://doi.org/10.1029/2009JA014394

Holme, R., 2000. Modelling of attitude error in vector magnetic data: application to Ørsted data. Earth, Planets and Space 52, 1187–1197. https://doi.org/10.1186/BF03352351

Holme, R., Bloxham, J., 1996. The magnetic fields of Uranus and Neptune: Methods and models. Journal of Geophysical Research: Planets 101, 2177–2200. https://doi.org/10.1029/95JE03437

Holme, R., Bloxham, J., 1995. Alleviation of the Backus Effect in geomagnetic field modelling. Geophysical Research Letters 22, 1641–1644. https://doi.org/10.1029/95GL01431

Hubbard, W.B., MacFarlane, J.J., 1980. Structure and evolution of Uranus and Neptune. Journal of Geophysical Research: Solid Earth 85, 225–234. https://doi.org/10.1029/JB085iB01p00225

Hunter, J.D., 2007. Matplotlib: A 2D Graphics Environment. Comput. Sci. Eng. 9, 90–95. https://doi.org/10.1109/MCSE.2007.55

Kohlhase, C.E., Penzo, P.A., 1977. Voyager mission description. Space Sci Rev 21, 77–101. https://doi.org/10.1007/BF00200846

Langel, R.A., 1988. International Geomagnetic Reference Field revision 1987. Eos, Transactions American Geophysical Union 69, 557–558. https://doi.org/10.1029/88EO00146

Lowes, F., 1966. Mean-Square Values on Sphere of Spherical Harmonic Vector Fields. Journal of Geophysical Research 71. https://doi.org/10.1029/JZ071i008p02179

Lowes, F.J., 1974. Spatial Power Spectrum of the Main Geomagnetic Field, and Extrapolation to the Core. Geophysical Journal International 36, 717–730. https://doi.org/10.1111/j.1365-246X.1974.tb00622.x

Maus, S., 2008. The geomagnetic power spectrum. Geophysical Journal International 174, 135–142. https://doi.org/10.1111/j.1365-246X.2008.03820.x

Ness, N.F., Acuña, M.H., Behannon, K.W., Burlaga, L.F., Connerney, J.E.P., Lepping, R.P., Neubauer, F.M., 1986. Magnetic Fields at Uranus. Science 233, 85–89. https://doi.org/10.1126/science.233.4759.85

Ness, N.F., Acuña, M.H., Burlaga, L.F., Connerney, J.E.P., Lepping, R.P., Neubauer, F.M., 1989. Magnetic Fields at Neptune. Science 246, 1473–1478. https://doi.org/10.1126/science.246.4936.1473

Ness, N.F., Connerney, J.E.P., Lepping, R.P., Schulz, M., Voigt, G.-H., 1991. The magnetic field and megnetospheric configuration of Uranus., Uranus.

Nettelmann, N., Helled, R., Fortney, J., Redmer, R., 2012. New indication for a dichotomy in the interior structure of Uranus and Neptune from the application of modified shape and rotation data. Planetary and Space Science 77. https://doi.org/10.1016/j.pss.2012.06.019

Neuenschwander, B.A., Helled, R., 2022. Empirical structure models of Uranus and Neptune. Monthly Notices of the Royal Astronomical Society 512, 3124–3136. https://doi.org/10.1093/mnras/stac628

Russell, C.T., 1993. Magnetic fields of the terrestrial planets. Journal of Geophysical Research: Planets 98, 18681–18695. https://doi.org/10.1029/93JE00981

Shure, L., Parker, R.L., Backus, G.E., 1982. Harmonic splines for geomagnetic modelling. Physics of the Earth and Planetary Interiors 28, 215–229. https://doi.org/10.1016/0031-9201(82)90003-6

Uieda, L., Tian, D., Leong, W.J., Jones, M., Schlitzer, W., Grund, M., Toney, L., Fröhlich, Y., Yao, J., Magen, Y., Materna, K., Belem, A., Newton, T., Anant, A., Ziebarth, M., Quinn, J., Wessel, P., 2022. PyGMT: A Python interface for the Generic Mapping Tools. https://doi.org/10.5281/ZENODO.3781524

Wessel, P., Smith, W.H.F., 1991. Free software helps map and display data. Eos, Transactions American Geophysical Union 72, 441–446. https://doi.org/10.1029/90EO00319

Web references:

Lepping, R.J., 1993. VG2-U-POS-5-SUMM-U1COORDS-48SEC-V1.0, VG2 URA TRAJECTORY DERIVED SUMM U1 COORDS 48SEC V1.0, [WWW Document]. NASA Planetary Data System, 1993. URL https://pds.nasa.gov/ds-view/pds/viewDataset.jsp?dsid=VG2-U-POS-5-SUMM-U1COORDS-48SEC-V1.0 (accessed 4.8.23).

Ness, N.F., 1993. PDS: Data Set Information Uranus [WWW Document]. URL https://pds.nasa.gov/ds-view/pds/viewProfile.jsp?dsid=VG2-U-MAG-4-RDR-U1COORDS-1.92SEC-V1.0 (accessed 2.2.23).

Ness, N.F., 1989. PDS: Data Set Information Neptune [WWW Document]. URL https://pds.nasa.gov/ds-view/pds/viewProfile.jsp?dsid=VG2-N-MAG-4-SUMM-NLSCOORDS-12SEC-V1.0 (accessed 2.2.23).

Appendix A:

Several Python Notebooks have been used to format the data from the NASA PDS (Planetary Data System) available: https://pds.nasa.gov/. Processed data files have been exported to MobaXterm for further analysis.
This can be found in the "Python code" folder attached.

A.1 Data:

The format for respective data files are to be constrained into 14 distinct columns, in order: Decimal descriptor, Latitude (degrees), West - Longitude (degrees), S/C distance from planet (Planetary Radii), number of data (here, 3), field north component, North Error, 1 (for x), field east component, East error, 2 (for Y), Field Down component, Down error, 3 (for Z).

Imports: Data imported to Python from Linux.
Exports: Data exported from Python to Linux.
Raw data as downloaded from NASAs PDS website is available in the "Python code/raw_data/" filepath.

A.2 Different Rotational Periods:

These files are available – labelled equivalent to "mfilename.txt" or "pfilename.txt" referring to "plus (+)" or "minus (-)" for different rotational periods, in minutes. These can be found in the path: "Python code/rotation/", there is a distinction between files that have constant longitude at the time of closest approach, or constant longitude at the start of the encounter. Constant longitude at closest approach is denoted by "fixed_ca" or equivalent.

A.3 Figures:

All generated figures throughout this project have been collated in the "figures" folder.

A.3 Jupyter Notebooks:

All notebooks have the extension: ".ipynb"

- “Creating_figures”: A collection of near all figures created in this dissertation.
- “Neptune”: Processing steps from raw data to exporting to MobaXterm.
- “Uranus”: Processing steps from raw data to exporting to MobaXterm.
- “pygmt”: Figures generated using PyGMT – separated because of conflicting packages in other Notebooks.
- “Richard”: Data processing and exporting of Richards Holme and Jeremy Bloxham’s ‘Udataraw’: dataset, and for direct comparisons to others.
- “Velocity”: Data processing to try and extract the velocity of Voyager 2 about the Uranus encounter.
- “constant_xyz”: Loading of misfits to data for both Uranus and Neptune, with the misfit to data being fixed at a constant residual value. Then the misfit to data for both planets when the smoothness is fixed.

A.4 Functions:

Found as the python file with extension “.py” – found “Python code/functions” – some of the python functions found in this file are used extensively within the Jupyter Notebooks. Such as the functions to alter the rotation rate, and export data to text files – the functions are appropriately described and commented to explain their purpose.